Enhancement of Power System Oscillation Damping of Single Machine Infinite Bus System by Incorporating Optimally Tuned Interline Power Flow Controller (IPFC)

by

Md. Moniruzzaman

MASTER OF SCIENCE

IN

ELECTRICAL AND ELECTRONIC ENGINEERING

Department of Electrical and Electronic Engineering
Islamic University of Technology (IUT)
Board Bazar, Gazipur-1704, Bangladesh
December 2019

CERTIFICATE OF APPROVAL

The thesis titled "**Enhancement of Power System Oscillation Damping of Single Machine Infinite Bus System by Incorporating Optimally Tuned Interline Power Flow Controller (IPFC)**" submitted by Md. Moniruzzaman, St. No. 142625 of Academic Year 2014-2015 has been found as satisfactory and accepted as partial fulfillment of the requirement for the Degree **of MASTER OF SCIENCE IN ELECTRICAL AND ELECTRONIC ENGINEERING** on 25 December 2019.

Board of Examiners:

1.

_____ Chairman

Dr. Ashik Ahmed (Supervisor)
Associate Professor,
Department of Electrical and Electronic Engineering
Islamic University of Technology (IUT), Gazipur.

2.

_____ Member

Dr. Md. Ruhul Amin
Professor and Head,
Department of Electrical and Electronic Engineering
Islamic University of Technology (IUT), Gazipur.

3.

_____

Dr. Golam Sarowar Member
Professor,
Department of Electrical and Electronic Engineering
Islamic University of Technology (IUT), Gazipur.

4.

_____ Member (External)

Dr. Md. Shahid Ullah
Professor,
Department of Electrical and Electronic Engineering
Daffodil International University, Ashulia, Savar, Dhaka.

Declaration of Candidate

It is hereby declared that this thesis report or any part of it has not been submitted elsewhere for the award of any Degree or Diploma.

_____

Dr. Ashik Ahmed
Associate Professor,
Electrical and Electronic Engineering Department,
Islamic University of Technology (IUT).
Date: 25 December 2019

_____

Md. Moniruzzaman
Student No.: 142625
Academic Year: 2014-15
Date: 25 December 2019

Dedicated to

"My Parents and Wife"

Table of Contents

Page No.

Chapter 3: Methodology

Chapter 4: Analysis of IPFC

Chapter 5: Conclusion and Future Scopes

List of Figures

List of Tables

List of Abbreviated Terms

DAE	Differential Algebraic Equation
DE	Differential Evolution
EM	Electromechanical Mode
FACTS	Flexible AC Transmission Systems
IPFC	Interline Power Flow Controller
ICA	Imperialist Optimization Algorithm
LFO	Low Frequency Oscillation
MPC	Model Predictive Control
MMPS	Multi Machine Power System
ODE	Ordinary Differential Equation
PSO	Particle Swarm Optimization
POD	Power Oscillation Damping
PSS	Power System Stabilizer
pu	per unit
RL	Reinforcement Learning
SMIB	Single Machine Infinite Bus
SSSC	Static Synchronous Series Compensator
STATCOM	Static Synchronous Compensator
SVC	Static VAR Compensator
SVD	Singular Value Decomposition
SVS	Synchronous Voltage Source
SFLA	Shuffled Frog Leaping Algorithm
TCSC	Thyristor Controlled Series Compensator
TCPS	Thyristor Controlled Phase Shifter
UPFC	Unified Power Flow Controller
VSC	Voltage Source Converter

Nomenclature

$\Delta V_1, \Delta V_2$	Injected voltage in line-1, 2
ΔV_{dc}	DC voltage deviation
ΔV_{dcref}	Reference DC voltage deviation
$\Delta\omega$	Rotor speed deviation
ΔE_{fd}	Field voltage deviation
δ	Rotor angle
θ_1, θ_2	Phase angle modulation index for VSC-1, 2
ω	Rotor speed
ω_b	Synchronous speed
C_{dc}	DC link capacitor of IPFC
D	Damping co-efficient of generator
d, q	Direct and quadrature axes
$E_q^{'}$	q-axis internal transient voltage
E_{fd0}	Initial field voltage
I_1, I_2	Current of transmission line-1, 2
I_{1d}, I_{2d}	d-axis current of transmission line-1, 2
I_{1q}, I_{2q}	q-axis current of transmission line-1, 2
I_d, I_q	d, q axes armature current
K_A, T_A	Gain, time constant of excitation system
k_{dc}	Proportional gain of controller
M	Inertia co-efficient of generator
m_1, m_2	Amplitude modulation index for VSC-1, 2
P_m, P_e	Mechanical input, electrical output power of generator
$T_{do}^{'}$	Open circuit field time constant
T_w, T_1, T_2	Washout, lead, lag time constant of controller
V_t	Generator terminal voltage
V_{dc}	DC link voltage of IPFC
V_1, V_2	Output voltage of VSC-1, 2

V_s	Nominal bus voltage
V_{ref}	Reference voltage
V_r	Infinite bus voltage
V_{rm}	Magnitude of infinite bus voltage
$x_d^{'}$	d-axis transient reactance
x_{l1}, x_{l2}	Reactance of transmission line-1, 2
x_d, x_q	d, q axes synchronous reactance
x_t	Transformer reactance
x_{t1}, x_{t2}	Reactance of VSC-1, 2 transformers

ACKNOWLEDGEMENT

First of all the praise is expressed to the Almighty Allah for keeping alive and able, giving the knowledge, ability to think and for helping to successfully finish this thesis. The author expresses deep gratefulness, thankfulness, appreciation to honorable teacher, respected supervisor Dr. Ashik Ahmed for continuous assistance, inspiration, guidance and valuable suggestions throughout the period of research. The author would like to extend deep sense of gratitude to all of the respective teachers of the Department of Electrical and Electronic Engineering, IUT for their valuable suggestions, cooperation and best wishes.

Finally, the author acknowledges that this work would be almost impossible to carry out successfully without the inspirations from parents and wife as they give moral support, optimistic encouragement throughout the research work.

Md. Moniruzzaman

25 December 2019

ABSTRACT

In power transmission system, low frequency oscillation (LFO) is created due to lack of balancing mechanical input to electrical output. For solving the LFO problem FACTs devices are being adopted. In this research work, as a FACTS device the Interline Power Flow Controller (IPFC) is employed. The IPFC based damping controller (Lead-Lag) has been used for mitigating LFO in single machine infinite bus (SMIB) system. An eigenvalue analysis is performed to select the electromechanical (EM) oscillation mode which is known as unstable mode. The controllability index is applied to select the most effective control signal of the controller. Since improper tuning of gain and time constants of controller called controller parameters may lead to sub-optimal result, particle swarm optimization (PSO) and differential evolution (DE) have been applied to tune the parameters. To investigate the effectiveness of the optimizers, the eigenvalue analysis and time-domain simulations are carried out. The quantitative analysis and nonparametric statistical tests have been performed to find out the most suitable optimizer for the controller. The results analysis reveals that the DE tuned Lead-Lag based damping controller for IPFC shows superior performance in damping LFOs for the study system.

Chapter 1

Introduction

In this chapter, an overview of the thesis is presented that demonstrates the inspiring behind this work. The concurrent and previous technology adopted to mitigate Low Frequency Oscillation (LFO) which is the main part of this research work has been markedly focused in this chapter. The background of research is illustrated in section 1.1. In article 1.2, the existing mitigating method of LFO has been discussed. In section 1.3, literature review is mentioned. Then the main objective of the research work has been illustrated in article 1.4. Finally the chapter is ended with hints of thesis outline in section 1.5.

1.1 Background

A primary complexity with producing and using electric energy is that it cannot be stored except fewer amounts for short periods of time. So, at a certain instant the production and consumption must be equal. To maintain the balance between power production and consumption, the generated energy of power stations has to be controlled continuously. When an imbalance is occurred, the frequency must be changed. At normal operating condition of power grid, the frequency is kept around a pre-set value, although permitted to fluctuate within a certain range. However, the main reason of frequency fluctuations is random demand changes and the nature of fluctuations is influenced by the state of the generators that are participating in control system. The oscillations related with groups of generators; oscillating against each other are known as inter-area oscillation modes that bound from 0.1 to 0.8 Hz and the oscillations related with only one generator; oscillating against rest of the system are known as local oscillation modes that bound from 0.7 to 2 Hz [1]. The both oscillations modes are commonly called low frequency oscillations (LFO) which hamper the power flow of the system, threaten system security and disturb smooth operation of the power system. To overcome these problems, it is very important to use controllers for providing sufficient damping to maintain the system stability [3].

In recent year, Flexible AC Transmission System (FACTS) devices are employed for enhancing power system stability. The FACTS devices became more effective and popular due to the advancement of power electronics. Mainly two types of FACTS - thyristor based FACTS and

Voltage Source Converter (VSC) based FACTS are used in practice. The latter family is more familiar because of its provision to use modern technology, operating features, and performance [9]. There are many VSC-based FACTS controller such as Static Synchronous Compensator (STATCOM) for shunt reactive power compensation, Static Synchronous Series Compensator (SSSC) for series reactive power compensation, Unified Power Flow Controller (UPFC) capable of compensating both active and reactive power independently, and Interline Power Flow Controller (IPFC) which is the main concern of this thesis [7, 8]. IPFC can regulate active and reactive power flows between different transmission lines by injecting series voltage into them and power transfer from overloaded to underloaded lines [6].

1.2 The existing mitigating method of LFO

Last few eras, Power System Stabilizer (PSS) has been extensively used to mitigate LFO, to improve the power system stability in an effective and economic way [11]. However, inability to mitigate voltage fluctuation, introduction of leading power factor, and failure to handle severe faults (i.e. three phase faults) are few of the major shortcomings of PSS which encourage the researchers to hunt for new damping controllers. Fortunately, with the advancement in power electronics based fast-switching elements; application of FACTS devices has become widespread with its excellent features of operation, controllability and transfer limits [12, 13], which motivates the researchers to employ FACTS devices in power system domain for enhancement of the stability. Although, at the beginning, thyristor based controller such as Static VAR Compensator (SVC), Thyristor Controlled Series Compensator (TCSC), Thyristor Controlled Phase Shifter (TCPS) are widely used for mitigating LFO; due to their slow response in terms of controllability, they have been recently replaced by new generation VSC based FACTS controller such as STATCOM, SSSC, UPFC and IPFC [13]. Among the last generation FACTS controllers using the self-commutated VSC [15], UPFC and IPFC are the most versatile and powerful devices, improving the transfer capability of existing transmission lines. The UPFC, combining the functions of the shunt and series compensation is capable to control the active and reactive power flows in the transmission line [16]. The IPFC with two or more series connected converters working together is conceived for the compensation of multi-line transmission system. Therefore, the power optimization of the overall system can be realized in the form of

appropriate power transfer from overload to under loaded lines, enhancement of transient stability and mitigation of system oscillations [17, 19].

1.3 Literature review

In this article, it describes several methods and controlling techniques to mitigate LFO in past and current researches. The efficiency of LFO mitigation generally depends on the effective design of damping controller. Hence, researchers' emphasis on the aspects of designing damping controller and the selection of the control strategy that is cited in many literatures has been included in this chapter. This section begins with the discussion of several famous research works on IPFC based damping controller for the improvement of LFO.

1.3.1 Research work based on IPFC equipped system relating to LFO and power flow

A substantial number of research works have been accomplished relating to small signal stability to reduce the problem associated with LFO. With this purpose, this research concentrates on the improvement of damping function and designing of damping controller for mitigating LFO. In recent years, there has been growing interest on studying IPFC modeling for mitigating LFO and controlling power flow among transmission lines.

A new IPFC steady-state model is presented in [2]. Where proposed an IPFC model that is equipped with power flow software. It proposes a scope of auto adjustment of IPFC parameters, counts of its operating bounds and stores all data in its memory. A case-study has been mentioned to show the performance of proposed IPFC model.

The modeling and simulation of a Single Machine Infinite Bus (SMIB) system integrated with IPFC based damping controller has been introduced in [4]. Where the performance of IPFC based stabilizing controller for enhancement the system stability have been presented. Particle Swarm Optimization (PSO) has been used to find out the optimal settings of controller parameters using different modulating signals. The most effective signals are selected with the help of controllability index. Although, this work presents the eigenvalues and nonlinear time domain simulation has been used to verify the effectiveness of IPFC based damping controller, this work has some limitations. Firstly, there is no comparative study of optimization. Secondly, the performance of different disturbances is not mentioned in this work. However, this works lacks of supportive analysis in favor of the robust damping controller.

In IPFC, two VSCs are connected by a dc capacitor for exchanging real power between two transmission lines. One of VSCs can capable of providing controlled series reactive power compensation by controlling magnitude and phase angle of VSC. Furthermore, it can able to control the transferred real power between lines through dc terminal. The IPFC enhance the power system stability and robust control of power flow in transmission lines [30].

An adaptive design of IPFC has been proposed in [10]. Where used reinforcement learning (RL) technique for damping of LFOs in power system. The RL based damping controller is integrated to SMIB and multi machine power system (MMPS). The proposed controller is capable of exhibiting its robustness and adaptive behavior against changing operating conditions with high nonlinearities in practical power system. To investigate the performance of the damping controller in both SMIB and MMPS, nonlinear simulations are carried out using MATLAB Simulink. The simulations are done the system integrated with (a) only optimal classical PSS, (b) coordinated designed of PSS and IPFC, and (c) RL based optimized IPFC. Krill herd optimization algorithm is used for coordination design of PSS and IPFC in both SMIB and MMPS. The performances in various operating conditions and fault types are examined for all 3 cases of simulations and are compared with one another. Simulation results show the effectiveness of the proposed damping controller to mitigate the LFOs in the power systems.

A SMIB system included with IPFC and PSS controller has been addressed. For improvement of system stability in various disturbances, a lead-lag controller has been proposed to produce supplementary signal. The proposed supplementary controller is applied to increase the damping of the power system LFOs. Imperialist optimization algorithm (ICA) and shuffled frog leaping algorithm (SFLA) are implemented to search for optimal controllers and PSS parameters. Moreover, singular value decomposition (SVD) method is utilized to select the most effective damping control signal of IPFC lead-lag controllers [27].

From the literature review of previous and existing models of IPFC based damping controller, it can be identified that there are some limitations.

- Some works concentrate on the basic design of damping controller but the optimization of the controller parameters is neglected.
- In some research works, optimization is used but quantitative and non-parametric statistical analysis missing.

To overcome these limitations, PSO & DE optimizers are employed in this work. For comparing the performance of the optimizers, quantitative and non-parametric statistical analyses are performed.

1.4 Research objectives

The treatment of the above-mentioned problems, a broadly adopted conventional controller is employed such as lead-lag controller to IPFC equipped SMIB system. Further, two different optimizers such as differential evolution (DE) and PSO are implemented to find out optimal gain for the controller. Later, we perform non-parametric statistical test to validate the effectiveness of each algorithms. In summary, the objective of this research work is given as follows:

i. To study a nonlinear dynamic model of an SMIB system integrated with IPFC.
ii. To analyze the system small signal stability of the linearized model in open-loop condition and incorporate controller.
iii. To tune the controller parameters using meta-heuristic optimization algorithms to find the optimal parameters.
iv. To study the dynamics of power system followed by small perturbation in time domain simulation.
v. To compare the performance of the optimizers using statistical tool, time domain simulation and eigenvalue analysis to realize optimal condition.

1.5 Thesis outline

Summary of this thesis work is organized as follows:

- Chapter 1 contains background, the existing mitigating method of LFO, literature review, research objectives and thesis outline.
- Chapter 2 describes the FACTS devices and mathematical model of IPFC.
- Chapter 3 explains the detailed methodology of proposed research work.
- Chapter 4 demonstrates the analysis of IPFC such as controllability test analysis in open loop system, eigenvalue analysis in close-loop system, time domain simulation with results, quantitative analysis and Non-Parametric statistical analysis.
- Chapter 5 is the last part of this research work which is ended with an explanatory conclusion with future work.

Chapter 2

FACTS Devices and Mathematical Model of IPFC

This chapter introduces the basic concepts of FACTS devices and mathematical model of IPFC equipped SMIB system. In the organization of this chapter, section 2.1 starts with introduction of FACTS devices. Section 2.2 depicts the basic elements of IPFC. Section 2.2.1 and 2.2.2 describe the basic construction and function of SSSC and IPFC respectively. The operation and control strategy of IPFC is discussed in section 2.3. In section 2.4, the nonlinear dynamic model of IPFC integrated SMIB system is described. This chapter is ended with the illustration of linearized model of IPFC integrated SMIB system in section 2.5.

2.1 Introduction of FACTS devices

For last several decades with the advancement of power electronics devices, application of FACTS devices has become simple with its excellent features of operations, controllability and transfer limits [5]. Turn of the century, to strengthen the power system, the technology of FACTS controller was advanced. Basically, FACTS devices are the power electronics-based controllers that are generally used with power transmission system to control one or more parameters of the system. There are many FACTS controllers, such as TCSC, SVC, SSSC and STATCOM. Combination of SSSC makes IPFC whereas a combination of SSSC and STATCOM forms UPFC. Although the FACTS controllers are costly than the ordinary power system controllers, they have been introduced in numerous real power system on the world

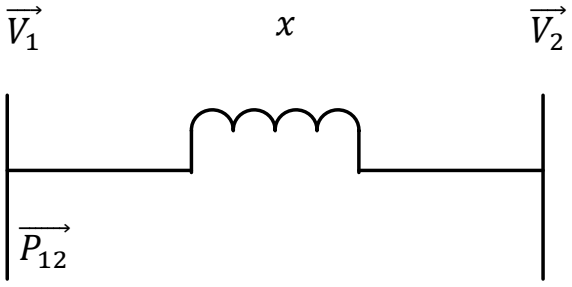

Figure 2.1: Circuit diagram for the illustration of operational principle of FACTS controllers

in order to their prevalent control execution capability [24]. Indeed, in order to regulate line power flow and to improve voltage profile, mechanically controlled series and shunt capacitors

were used since the beginning of FACTS devices as early as the 1920s. The application of power electronics devices was prevalent when mercury valve was replaced by thyristor in controlling high voltage DC systems. The new age of FACTS controllers utilizes self-commutated, voltage source based power converters to realize quickly controllable, static synchronous AC voltage or current sources. Another age FACTS controller is built essentially on the synchronous voltage source (SVS) which is a perfect machine with no rotation and inertia. The magnitude and phase of the SVS can be controlled instantly to create reactive power as well as to direct active power flow that is not influenced by the variables affecting power flow [30]. The fundamental principle of the FACTS controllers can be described by the Fig.2.1 [31]. The real power transferred along the transmission line is expressed as following:

$$\overrightarrow{P_{12}} = \frac{\overrightarrow{V_1}\,\overrightarrow{V_2}}{x} sin\theta \qquad (2.1)$$

Where, θ is the phase angle difference between the sending end voltage, $\overrightarrow{V_1}$ and the receiving end voltage, $\overrightarrow{V_2}$ of the transmission line. In order to control power flow along the transmission lines it is essential for a FACTS controller to change the line impedance x with time, the magnitude of line voltages ($\overrightarrow{V_1}, \overrightarrow{V_2}$), and phase angle separately to such a range that superior adaptability of power flow management is accomplished [32, 33].

2.2 Basic elements of IPFC

The IPFC consists of two or more SSSCs. The common feature of IPFC is the possibility to exchange active and reactive power between transmission lines. To understand the comprehensive model of IPFC, it should be realize its basic elements. The basic element of IPFC is SSSC that use VSC based converter. The basic block diagram and function of these elements are shown in Fig. 2.2.

2.2.1 Static Synchronous Series Compensator (SSSC)

The SSSC is a combination of a dc source, a VSC (converts dc voltage into 3-ϕ output voltage at fundamental frequency), and a coupling transformer that is shown in Fig.2.2. It is connected in series with the power transmission line. The SSSC injects a voltage into the line in quadrature to the line current, thus emulating an inductive or a capacitive reactance in series with the line. The

SSSC operates like a controllable series capacitor and series inductor. Then the power flow on the line can be affected through the control of this series reactance. Thus the SSSC is capable of supplying or absorbing reactive power in the line [41].

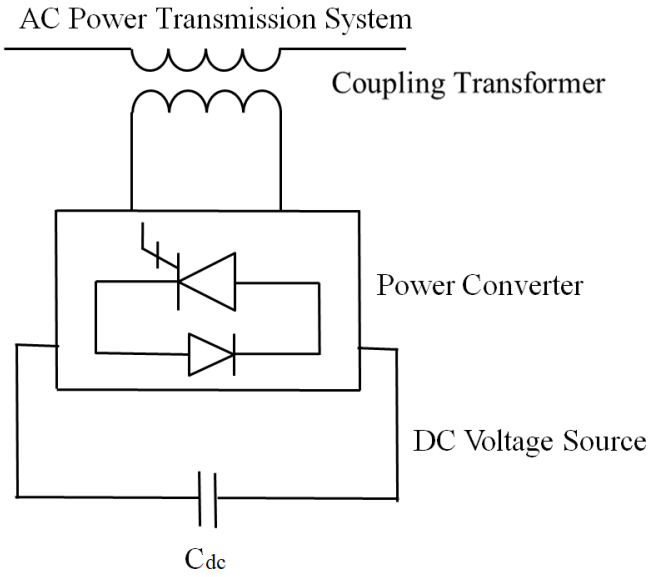

Figure 2.2: Schematic diagram of SSSC

2.2.2 Interline Power Flow Controller (IPFC)

The IPFC topology is shown in Fig.2.3. A series VSC is inserted into each of several transmission lines, with all VSCs sharing a common dc link. In the IPFC both VSCs exchange active power with their power transmission lines. However, the active power injected by one power converter to its power transmission line must be equal (neglecting losses) to the active power taken away from the other power transmission line. The IPFC makes it possible to equalize real and reactive power flow between power transmission lines. It allows transferring power from overloaded transmission line to underloaded line.

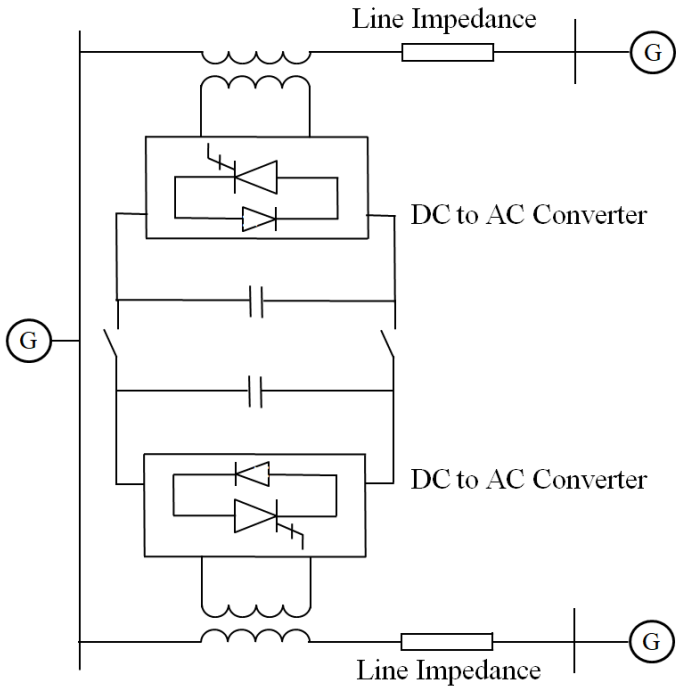

Figure 2.3: Schematic diagram of IPFC

2.3 Operation and control strategy of IPFC

The IPFC is a controller that can control both active and reactive powers between the transmission lines, that means the phase angle and magnitude of voltage are controllable. It made of two or more series connected converters supplied by a common DC link, which enables the IPFC to compensate multiple transmission lines. The basic operation principle of an IPFC was described in [14]. A schematic diagram of the IPFC is shown in Fig. 2.3, which employs two back-to-back dc-to-ac converters that are connected in series with two transmission lines via series coupling transformers and the dc terminals of two inverters are connected through a common DC link. Finally it acts as an ac to ac converter.

The equivalent circuit of an IPFC is shown in Fig. 2.4. Here, V_S and δ_s denotes the magnitude and phase angle of sending end voltage respectively; whereas V_{1r} and δ_{1r} denotes the magnitude and phase angle of receiving end voltage of transmission line-1 respectively; ΔV_1 and ψ_1 denotes the magnitude of injected voltage and corresponding phase angle respectively; R_1 and X_1 represent resistance and reactance of transmission line-1 respectively. Using Kirchhoff's Voltage Law it is obtained as follows.

$$V_s\angle\delta s \pm \Delta V_1\angle\psi 1 - I_1\angle\gamma 1(R_1 + jX_1) - V_{1r}\angle\delta 1r = 0 \qquad (2.2)$$

$$I_1\angle\gamma 1 = \frac{V_s\angle\delta s \pm \Delta V_1\angle\psi 1 - V_{1r}\angle\delta 1r}{R1 + jX1} \quad (2.3)$$

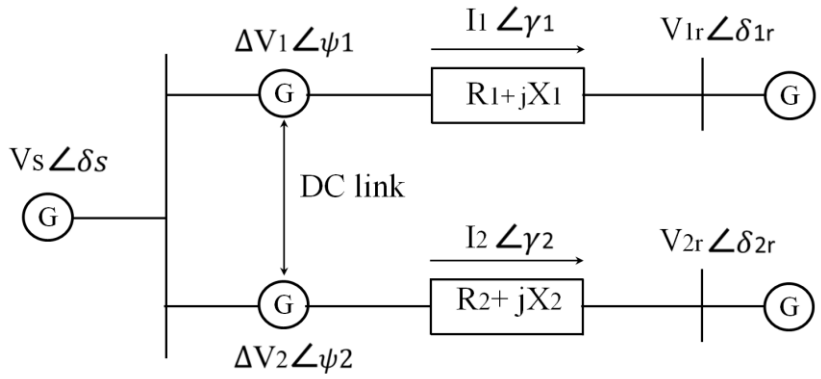

Figure 2.4: Equivalent circuit of IPFC with its variables

In fig. 2.5 shows the open loop model of IPFC equipped SMIB system. In this model, the transmission line represents as a lossless line, so resistance is neglected. Here, x_d and x_q denotes the d and q axes synchronous reactance of generator; x_d' denotes d axis transient reactance of generator; V_t represents generator terminal voltage; x_t express reactance of line transformer; x_{t1} and x_{t2} denotes reactance of VSC-1 and VSC-2 transformers; x_{l1} and x_{l2} presents reactance of transmission line-1 and line-2; V_1 and V_2 denotes output ac voltage of VSC-1 and VSC-2 respectively. There are four controllable signals such as m_1, θ_1 are input to VSC-1 and m_2, & θ_2 are input to VSC-2. The injection or absorption of active or reactive power to transmission line-1is regulated by modulation index (m_1) & phase angle (θ_1) and that of transmission line-2 is regulated by modulation index (m_2) & phase angle (θ_2) respectively.

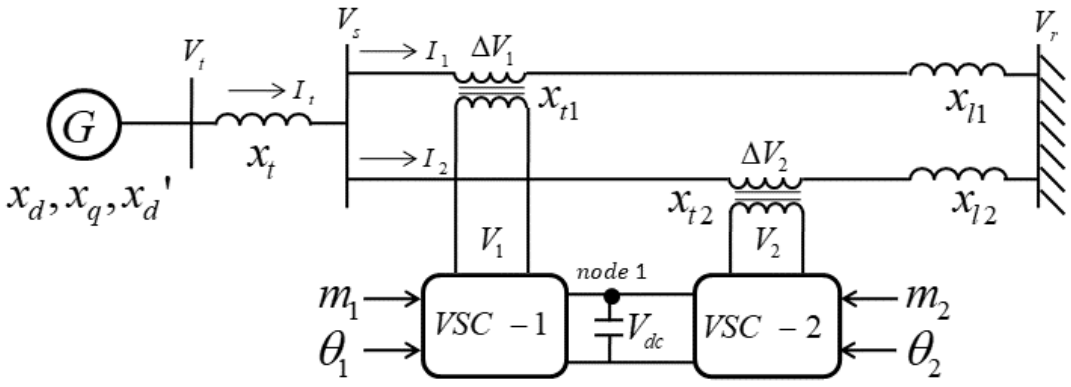

Figure 2.5: Open loop model of IPFC equipped SMIB system

2.4 Nonlinear dynamic model of IPFC integrated SMIB system

To represent this research work, the IPFC integrated SMIB system has been considered that is shown in Fig. 2.5. The main parts of the system are a generator, a transformer, two parallel transmission lines and IPFC. The transients and resistance of transformer has been neglected for developing simplified non-linear differential equations. The differential equations are the function of the variables such as rotor speed (ω), rotor angle (δ), field voltage (E_{fd}), q-axis internal transient voltage (E'_q) and dc voltage (V_{dc}) that regulate the dynamic model of the IPFC equipped SMIB system. The equations are associated with the generator and its excitation system. The nonlinear dynamic model of generator and excitation system represents the effect of steady-state and direct (d) - quadrature (q) axes reactance's on overall system performance whenever the mitigation of LFO in power system is of prime goal [43]. Additionally, consideration of dynamic field excitation allows the capability of establishing regulate in generator terminal voltage. So, the dynamic model of generator and its excitation system have been considered for this work is expressed as follows.

$$\dot{\delta} = \omega_b(\omega - 1) \tag{2.4}$$

$$\dot{\omega} = \frac{1}{M}[P_m - P_e - D(\omega - 1)] \tag{2.5}$$

$$\dot{E}'_q = \frac{1}{T'_{d0}}[E_{fd0} + \Delta E_{fd} - E'_q - (x_d - x'_d)I_d] \tag{2.6}$$

$$\Delta\dot{E}_{fd} = \frac{1}{T_A}[K_A(V_{ref} - V_t)\Delta E_{fd}] \tag{2.7}$$

Where,

ω_b = synchronous speed

M = inertia co-efficient of generator

P_m = mechanical input power of generator

P_e = electrical output power of generator

D = damping co-efficient of generator

T'_{do} = open circuit field time constant

E_{fd0} = initial field voltage

ΔE_{fd} = field voltage deviation

x_d = d-axis synchronous reactance

x'_d = d-axis transient reactance

I_d = d-axis armature current

T_A = time constant of excitation system

K_A = gain constant of excitation system

V_{ref} = reference voltage

V_t = generator terminal voltage

The equations (3.1-3.4) represent the dynamic state equations of third order generator model [18].

Where,

The output power of generator, $P_e = V_{td}I_{td} + V_{tq}I_{tq}$

The terminal voltage of generator, $V_t = V_{td} + jV_{tq}$

d-axis terminal voltage of generator, $V_{td} = X_q.I_{tq}$

q-axis terminal voltage of generator, $V_{tq} = E'_q - X'_d.I_{td}$

d-axis terminal current of generator, $I_{td} = I_{1d} + I_{2d}$

q-axis terminal current of generator, $I_{tq} = I_{1q} + I_{2q}$

The terminal current of generator, $I_t = I_1 + I_2$ or, $I_t = I_{td} + jI_{tq}$

The current of transmission line-1, $I_1 = I_{1d} + jI_{1q}$

The current of transmission line-2, $I_2 = I_{2d} + jI_{2q}$

As the IPFC is linked into SMIB system, the dc-link voltage dynamics of IPFC is obtained by using Kirchhoff's Current Law at node 1 mentioned in Fig 2.5, which can be shown by the following equation [27].

$$\dot{V}_{dc} = \frac{0.5m_1}{C_{dc}}\left[I_{1d}\cos\theta_1 + I_{1q}\sin\theta_1\right] + \frac{0.5m_2}{C_{dc}}\left[I_{2d}\cos\theta_2 + I_{2q}\sin\theta_2\right] \quad (2.8)$$

Where,

m_1, m_2 = amplitude modulation index for VSC $-$ 1, 2

I_{1d}, I_{2d} = d $-$ axis current of transmission line $-$ 1, 2

I_{1q}, I_{2q} = q $-$ axis current of transmission line $-$ 1, 2

θ_1, θ_2 = phase angle modulation index for VSC $-$ 1, 2

C_{dc} = dc link capacitor of IPFC

The equation of generator terminal voltage is obtained by applying Kirchhoff's Voltage Law on generator terminal to transmission line-1 in Fig. 2.5 as follows.

$$V_t = jx_t I_t - \Delta V_1 + jx_{l1} I_1 + V_r$$

$$\text{or, } V_{td} + j\,V_{tq} = jx_t(I_{td} + jI_{tq}) - (\Delta V_{1d} + j\,\Delta V_{1q}) + jx_{l1}(I_{1d} + j\,I_{1q}) + V_{rm}(sin\delta + jcos\delta) \quad (2.9)$$

Where,

x_t = transformer reactance

ΔV_1 = injected voltage in line $-$ 1

x_{l1} = reactance of line $-$ 1

V_r = infinite bus voltage

V_{rm} = magnitude of infinite bus voltage

$\Delta V_{1d}, \Delta V_{1q}$ = d, q axes injected voltage in line $-$ 1

The resistances of the IPFC transformers are ignored and per unit values of three phase dynamic differential equations of IPFC are obtained as follows [27].

As VSC-1 associated with transmission line-1,

$$\Delta V_1 = jx_{t1} I_1 + 0.5 V_{dc} m_1 e^{j\theta_1}$$

$$\text{Or, } \Delta V_{1d} + j\Delta V_{1q} = jx_{t1}(I_{1d} + jI_{1q}) + 0.5 V_{dc} m_1 (cos\theta_1 + jsin\theta_1) \quad (2.10)$$

The following equations are obtained by equating real and imaginary part of equation (2.10),

$$\Delta V_{1d} = -x_{t1} I_{1q} + 0.5 V_{dc} m_1 cos\theta_1 \quad (2.11)$$

$$\Delta V_{1q} = jx_{t1} I_{1d} + 0.5 V_{dc} m_1 sin\theta_1 \quad (2.12)$$

As VSC-2 associated with transmission line-2,

$$\Delta V_2 = jx_{t2} I_2 + 0.5 V_{dc} m_2 e^{j\theta_2}$$

$$\text{Or, } \Delta V_{2d} + j\Delta V_{2q} = jx_{t2}(I_{2d} + jI_{2q}) + 0.5 V_{dc} m_2 (cos\theta_2 + jsin\theta_2) \quad (2.13)$$

The following equations are obtained by equating real and imaginary part of equation (2.13),

$$\Delta V_{2d} = -x_{t2} I_{2q} + 0.5 V_{dc} m_2 cos\theta_2 \quad (2.14)$$

$$\Delta V_{2q} = jx_{t2} I_{2d} + 0.5 V_{dc} m_2 sin\theta_2 \quad (2.15)$$

By solving the above equations (2.11, 2.12, 2.14 & 2.15), the following relations in matrix form are obtained.

$$\begin{bmatrix} I_{1q} \\ I_{2q} \end{bmatrix} = \begin{bmatrix} \frac{x_{22}}{x_{dq}} & -\frac{x_{12}}{x_{dq}} \\ -\frac{x_{21}}{x_{dq}} & \frac{x_{11}}{x_{dq}} \end{bmatrix} \begin{bmatrix} -0.5 m_1 V_{dc} cos\theta_1 + V_{rm} sin\delta \\ 0.5 m_2 V_{dc} cos\theta_2 - 0.5 m_1 V_{dc} cos\theta_1 \end{bmatrix} \quad (2.16)$$

$$\begin{bmatrix} I_{1d} \\ I_{2d} \end{bmatrix} = \begin{bmatrix} \frac{x_{22}}{x_{dd}} & -\frac{x_{12p}}{x_{dd}} \\ -\frac{x_{21}}{x_{dd}} & \frac{x_{11d}}{x_{dd}} \end{bmatrix} \begin{bmatrix} E'_q + 0.5m_1 V_{dc} \sin\theta_1 - V_{rm}\cos\delta \\ 0.5 m_2 V_{dc} \sin\theta_2 - 0.5 m_1 V_{dc} \sin\theta_1 \end{bmatrix} \quad (2.17)$$

Where,

$x_{12} = x_t + x_q$

$x_{21} = -x_{t1} + x_{l1}$

$x_{11} = x_{12} + x_{21}$

$x_{22} = x_{t2} - x_{l2}$

$x_{12p} = x_t + x'_d$

$x_{11d} = x_{12p} + x_{21}$

$x_{dq} = x_{11}x_{22} - x_{12}x_{21}$

$x_{dd} = x_{22}x_{11d} - x_{21}x_{12p}$

In next section, the linearized system matrix is formulated from this mathematical expressions of nonlinear dynamic model of IPFC equipped SMIB system to perform eigenvalue and participation factor analysis for open-loop condition [46].

2.5 Linearized Model of IPFC Integrated SMIB System

Here, the linearization technique is applied on the non-linear dynamic model for developing linearized form for each consequent dynamic mathematical equation (2.4-2.8), since this linearized model is suitable for analysis of small signal stability [48]. For this target, the Taylor series expansion is employed to these non-linear mathematical equations and removes the higher order term for obtaining linearized equations. It is well known that removal of higher order term will sacrifice some accuracy, since non-linearities associated with terms are being ignored [44]. However, the small perturbation is considered for this work, linearized mathematical representation of this system dynamic model is considerably correct [45]. Now, Taylor series expansion is applied to non-linear dynamic equations (2.4-2.8) and the following linearized equations are obtained for considering first order term.

$$\Delta\dot{\delta} = \omega_b \Delta\omega \quad (2.18)$$

$$\Delta\dot{\omega} = \frac{1}{M}[\Delta P_m - \Delta P_e - D\Delta\omega] \quad (2.19)$$

$$\Delta\dot{E}_q^{'} = \frac{1}{T_{do}^{'}}\left[\Delta E_{fd} - \Delta E_q\right] \tag{2.20}$$

$$\Delta\dot{E}_{fd} = \frac{1}{T_A}[K_A(\Delta V_{ref} - \Delta V_t) - \Delta E_{fd}] \tag{2.21}$$

$$\Delta\dot{V}_{dc} = K_7\Delta\delta + K_8\Delta E_q^{'} - K_9\Delta V_{dc} + K_{cm1}\Delta m_1 + K_{c\theta_1}\Delta\theta_1 + K_{cm2}\Delta m_2 + K_{c\theta_2}\Delta\theta_2 \tag{2.22}$$

where,

$$\Delta P_e = K_1\Delta\delta + K_2\Delta E_q^{'} + K_{pv}\Delta V_{dc} + K_{pm1}\Delta m_1 + K_{p\theta_1}\Delta\theta_1 + K_{pm2}\Delta m_2 + K_{p\theta_2}\Delta\theta_2 \tag{2.23}$$

$$\Delta E_q = K_3\Delta\delta + K_4\Delta E_q^{'} + K_{qv}\Delta V_{dc} + K_{qm1}\Delta m_1 + K_{q\theta_1}\Delta\theta_1 + K_{qm2}\Delta m_2 + K_{q\theta_2}\Delta\theta_2 \tag{2.24}$$

$$\Delta V_t = K_5\Delta\delta + K_6\Delta E_q^{'} + K_{vv}\Delta V_{dc} + K_{vm1}\Delta m_1 + K_{v\theta_1}\Delta\theta_1 + K_{vm2}\Delta m_2 + K_{v\theta_2}\Delta\theta_2 \tag{2.25}$$

This model has 28 “K” constants which are termed as linearized constants. It is prominent way is that the linearized form permits to represent the system using state space model. In general, the state space model is expressed as follows.

$$\dot{X} = AX + BU$$

Where,

$$\text{State Vector, } X = \left[\Delta\delta \;\; \Delta\omega \;\; \Delta E_q^{'} \;\; \Delta E_{fd} \;\; \Delta V_{dc}\right]^T$$

$$\text{Control Vector, } U = \left[\Delta m_1 \;\; \Delta\theta_1 \;\; \Delta m_2 \;\; \Delta\theta_2\right]^T$$

In general, A and B are known as system matrix and input matrix respectively. The matrices A and B help us to find out system eigenvalues, participation factor and controllability index for open loop condition [42]. Now, the equations (2.23 - 2.25) are substituted into the linearized equations (2.19 - 2.21) and the following state space equations of the IPFC integrated SMIB system are achieved.

$$\begin{bmatrix} \Delta\dot{\delta} \\ \Delta\dot{\omega} \\ \Delta\dot{E}_q^{'} \\ \Delta\dot{E}_{fd} \\ \Delta\dot{V}_{dc} \end{bmatrix} = \begin{bmatrix} 0 & \omega_b & 0 & 0 & 0 \\ \frac{-K_1}{M} & \frac{-D}{M} & \frac{-K_2}{M} & 0 & \frac{-K_{pv}}{M} \\ \frac{-K_3}{T_{do}^{'}} & \frac{0}{T_{do}^{'}} & \frac{-K_4}{T_{do}^{'}} & \frac{1}{T_{do}^{'}} & \frac{-K_{qv}}{T_{do}^{'}} \\ \frac{-K_AK_5}{T_A} & \frac{0}{T_A} & \frac{-K_AK_6}{T_A} & \frac{-1}{T_A} & \frac{-K_AK_{vv}}{T_A} \\ K_7 & 0 & K_8 & 0 & -K_9 \end{bmatrix} \begin{bmatrix} \Delta\delta \\ \Delta\omega \\ \Delta E_q^{'} \\ \Delta E_{fd} \\ \Delta V_{dc} \end{bmatrix} + \begin{bmatrix} 0 & 0 & 0 & 0 \\ \frac{-K_{pm_1}}{M} & \frac{-K_{p\theta_1}}{M} & \frac{-K_{pm_2}}{M} & \frac{-K_{p\theta_2}}{M} \\ \frac{-K_{qm_1}}{T_{do}^{'}} & \frac{-K_{q\theta_1}}{T_{do}^{'}} & \frac{-K_{qm_2}}{T_{do}^{'}} & \frac{-K_{q\theta_2}}{T_{do}^{'}} \\ \frac{-K_AK_{vm_1}}{T_A} & \frac{-K_AK_{v\theta_1}}{T_A} & \frac{-K_AK_{vm_2}}{T_A} & \frac{-K_AK_{v\theta_2}}{T_A} \\ K_{cm_1} & K_{c\theta_1} & K_{cm_2} & K_{c\theta_2} \end{bmatrix} \begin{bmatrix} \Delta m_1 \\ \Delta\theta_1 \\ \Delta m_2 \\ \Delta\theta_2 \end{bmatrix}$$

Where,

$$\text{System matrix, } A = \begin{bmatrix} 0 & \omega_b & 0 & 0 & 0 \\ \frac{-K_1}{M} & \frac{-D}{M} & \frac{-K_2}{M} & 0 & \frac{-K_{pv}}{M} \\ \frac{-K_3}{T'_{do}} & \frac{0}{T'_{do}} & \frac{-K_4}{T'_{do}} & \frac{1}{T'_{do}} & \frac{-K_{qv}}{T'_{do}} \\ \frac{-K_A K_5}{T_A} & \frac{0}{T_A} & \frac{-K_A K_6}{T_A} & \frac{-1}{T_A} & \frac{-K_A K_{vv}}{T_A} \\ K_7 & 0 & K_8 & 0 & -K_9 \end{bmatrix}$$

$$\text{Input matrix, } B = \begin{bmatrix} 0 & 0 & 0 & 0 \\ \frac{-K_{pm_1}}{M} & \frac{-K_{p\theta_1}}{M} & \frac{-K_{pm_2}}{M} & \frac{-K_{p\theta_2}}{M} \\ \frac{-K_{qm_1}}{T'_{do}} & \frac{-K_{q\theta_1}}{T'_{do}} & \frac{-K_{qm_2}}{T'_{do}} & \frac{-K_{q\theta_2}}{T'_{do}} \\ \frac{-K_A K_{vm_1}}{T_A} & \frac{-K_A K_{v\theta_1}}{T_A} & \frac{-K_A K_{vm_2}}{T_A} & \frac{-K_A K_{v\theta_2}}{T_A} \\ K_{cm_1} & K_{c\theta_1} & K_{cm_2} & K_{c\theta_2} \end{bmatrix}$$

Generally, A and B are used to explain the characteristics of a system. According to stability theory, it is well known that if anyone of the eigenvalues of A lies in the right of half s-plane, the system is said to be unstable and if anyone of the eigenvalues of A lies in the left of half s-plane, the system is said to be stable. A and B are the constant matrices with suitable dimensions which are dependent on the operating point of the system. As long as all eigenvalues have negative real parts, the power system is stable when it is subjected to a small disturbance. If one of these modes has a positive real part the system is unstable.

Chapter 3

Methodology

This chapter describes the basic method to investigate LFO generated due to various causes in electrical power system. In the organization of this chapter, section 3.1 discusses the open loop eigenvalue analysis method. Then, finding eigenvalues and eigenvectors are described in 3.1.1. The formation of participation factor matrix is explained in section 3.1.2. In section 3.1.3, represent the identification of unstable mode from the open-loop analysis. Section 3.2 depicts the identification of best control signal. The design of damping controller is discussed in section 3.3. Section 3.4 depicts the close-loop system construction. The optimization algorithms are described in section 3.5. Subsection 3.5.1 & 3.5.2 illustrate PSO & DE algorithms respectively. Section 3.6 explains the objective functions. The controller parameters optimization is discussed in section 3.7. Section 3.8 explains time domain analysis. The non-parametric statistical test is illustrated in section 3.9. This chapter is ended by the discussion of parameters of IPFC equipped SMIB system in section 3.10.

3.1 Open loop eigenvalue analysis

The eigenvalue analysis can be used to investigate the small signal stability of the system at running condition. The type of the oscillation can be recognized by the nature of eigenvalue. Also, the participation factor is formed by eigenvectors which are obtained from eigenvalues of the system matrix. The participation factors indicate the involvement of producing LFO. Again, the damping ratio and oscillation frequency are to be computed from the eigenvalues that can help for finding the effectiveness of damping controller. The information regarding the dominant state of the system matrix is calculated by participation matrix gives clear conception of the oscillatory mode. The fundamental steps to investigate the LFO are as follows.

- Step-1: To find equilibrium point
- Step-2: To perform linearization of the differential equation of the system model around the operating point
- Step-3: Transformation of differential algebraic equation (DAE) to ordinary differential equation (ODE) to form system matrix in reduced form

- Step-4: To find eigenvalues, eigenvectors and participation matrix

3.1.1 Finding eigenvalues and eigenvectors

With the help of system state matrix, it is easy to investigate the characteristics of steady state stability around the operating point. The number of states and eigenvalues depend on the dimension of the system matrix.

$$[\mathrm{A} - \lambda \mathrm{I}]\phi = 0 \tag{3.1}$$

Where λ represents eigenvalues and ϕ represents right eigenvector. For non-trivial solution determinant of $[\mathrm{A} - \lambda \mathrm{I}]$ equals to zeros and the eigenvalues can be calculated. Similarly, another equation can be written to find out the left eigenvector ψ as given below.

$$[\mathrm{A} - \lambda \mathrm{I}]\psi = 0 \tag{3.2}$$

The right eigenvector contains information how each of the system state is affected by the oscillatory mode. It also determines the observability of the system. The controllability of a system is determined by left eigenvector. Eigenvector is used to find participation factors. The eigenvalues of the system matrix must lie in the left half plane to make the system stable. This indicates that the real part of complex conjugate must be placed in the left half plane. For unstable system the real part of complex conjugate always lies in the right half plane [34].

Assume an eigenvalue in complex format, $\lambda = \sigma \pm j\omega$, the initial oscillation frequency (f) and damping ratio (ξ) can be calculated using the following expressions [47].

$$\xi = \frac{-\sigma}{\sqrt{\sigma^2 + \omega^2}} \tag{3.3}$$

$$f = \frac{\omega}{2\pi} \tag{3.4}$$

3.1.2 Formation of participation factor matrix

The participation factor matrix is formed by the left and right eigenvectors as following [35].

$$\mathrm{P} = [\, P_1, P_2, \ldots\ldots P_n \,] \tag{3.5}$$

$$\text{With } P_i = \begin{bmatrix} P_1 \\ P_2 \\ \cdots \\ P_n \end{bmatrix} = \begin{bmatrix} \phi_{1i}\psi_{i1} \\ \phi_{2i}\psi_{i2} \\ \cdots\cdots\cdots \\ \phi_{ni}\psi_{in} \end{bmatrix}$$

$$\text{Participation factor matrix, } P_{ki} = \phi_{ki}\psi_{ik} \tag{3.6}$$

Where, ϕ_{ki} = right eigenvector of i[th] mode and ψ_{ik} = left eigenvector of i[th] mode

3.1.3 Identification of unstable mode from open loop analysis

The eigenvalues provide stability information of the system. The electromechanical (EM) oscillation mode associated with machine inertia is found in eigenvalue analysis. The EM oscillation is related to the rotor speed equation of generators. The EM mode is identified by investigating the conjugate complex eigenvalue having higher participation factors than those of other state variables [30].

3.2 Identification of best control signal

The best control signal affects significantly on enhancing the damping of unstable EM oscillation ($\Delta\delta, \Delta\omega$) mode for the system. Hence, it is essential to identify the best control signal out of four ($m_1, \theta_1, m_2, \theta_2$) of IPFC to integrate it with SMIB system [37]. The controllability and observability index analysis are commonly used for choosing most effective control signal. The characteristic of controllability handles the control input for adjusting the system state to a desired one. The property of observability helps to determine the initial state whether it is observable from the output or not. It is impossible to find out the particular state behavior from the system output, unless it is observable; hence not suited to stabilize that state. The controllability and observability index are obtained from eigenvector corresponding to oscillatory mode. The controllability index is calculated using the following equations [38, 39].

$$r_{ki} = b_{ki}\, O_i \tag{3.7}$$

$$b_{ki} = W_i^T B_k \tag{3.8}$$

Here, i corresponds to the i[th] state of eigenvalue, which are 3 and 4 in this work, since they are associated with EM mode as illustrated in Table 4.1. Also, k = 1 . . . 4, column number of input matrix B; O_i is the observability index for corresponding EM modes. W_i^T is the left eigenvector

for EM modes of system matrix; A, B is the input matrix mentioned in linearization section. The result obtained from controllability index is presented in Fig. 3.1.

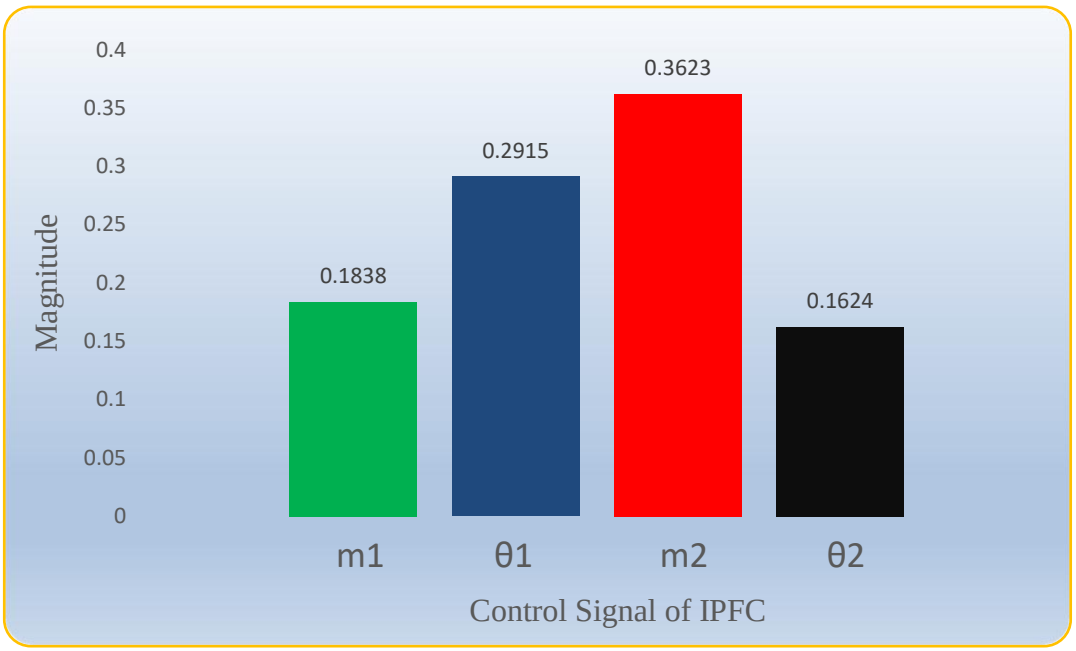

Figure 3.1: Controllability index among four control signals of IPFC

This figure describes that m_2 control signal has significant impact on the improvement of our negatively damped EM mode than other control signals of IPFC, since m_2 shows higher magnitude (0.3623) in controllability index. Hence, m_2 is considered as best control signal for controller design.

Table 3.1: Eigenvalues and participation factor analysis in open loop condition

Eigenvalue, $\lambda = \sigma \pm j\omega$	Associated state	Participation factor (%)	Damping ratio, $\xi = \frac{-\sigma}{\sqrt{\sigma^2+\omega^2}}$	Oscillation frequency, $f = \frac{\omega}{2\pi}$
-91.6101 + j0.0000	ΔE_{fd}	99.41%	1.0000	0.0000
-10.1923 + j0.0000	$\Delta E_q^{'}$	98.50%	1.0000	0.0000
0.3947 $\pm$ j6.5774	$\Delta\delta, \Delta\omega$	48.89%	-0.0599	1.0468
0.0203 + j 0.0000	ΔV_{dc}	99.91%	- 1.0000	0.0000

Furthermore, for describing the stability nature, open-loop condition has been examined that is presented in Table 3.1. It is observed that the unstable state is associated with the EM mode and

the corresponding damping ratio is -0.0599 with an oscillation frequency of 1.0468 Hz.

3.3 Design of damping controller

In case of small signal stability, when the system is subjected to a sudden fault then fluctuation occurs around the operating point that results in power oscillation. Unless adequate damping is provided to damp this power oscillation it leads to system failure.

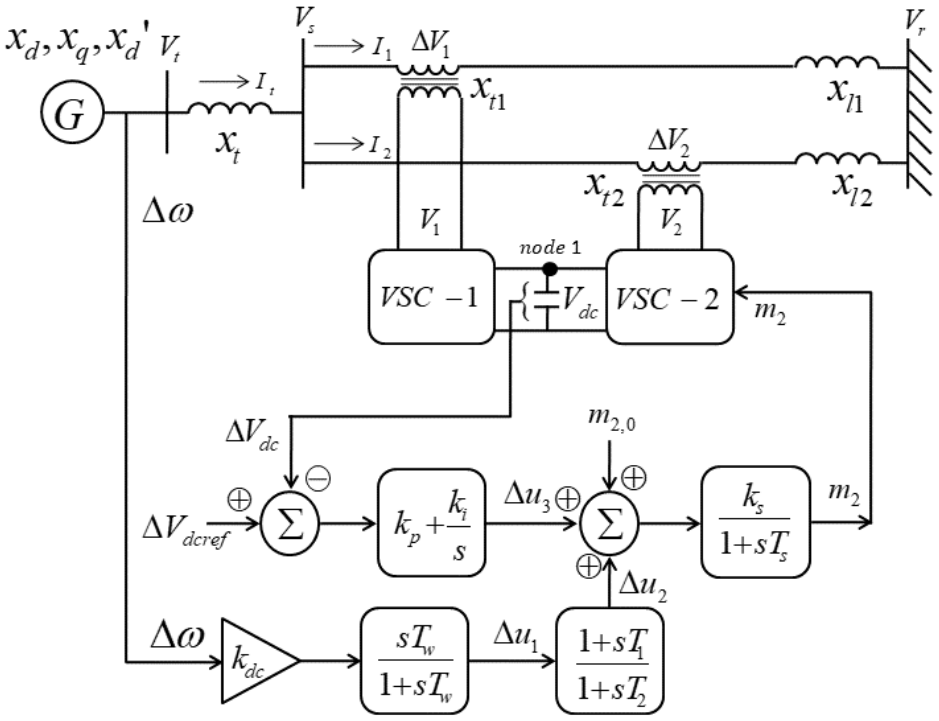

Figure 3.2: Close loop configuration of IPFC integrated SMIB system

For solving the power oscillation problem different supplementary controllers equipped with FACTS devices are used. In this work, the Lead-Lag controller applied to IPFC which is denoted as power oscillation damping (POD). To mitigate LFO, it must be increased system damping by diminishing EM oscillations. Hence POD control action is adopted in with IPFC. It is customary to place IPFC in the transmission line to regulate active or reactive power flow along the line and generally speed deviation ($\Delta\omega$) is preferred as input to the Lead-Lag controller of IPFC [27].

3.4 Close loop system construction

In order to construct close loop system, lead-lag controller is attached for obtaining the best control signal, m_2 in order to improve damping. The close loop system of this work is shown in Fig. 3.2. It is to be noted that, a voltage regulator is incorporated for maintaining dc link dynamics within tolerable limit, where it receives an error signal resulting from the comparison between actual dc link voltage (ΔV_{dc}) and corresponding reference voltage (ΔV_{dref}) to generate output signal, Δu_3. The lead-lag controller block receives speed deviation ($\Delta\omega$), processes it and deliver output signal, Δu_2. It is to be noted that the number of associated states with the controller is two ($\Delta u_1, \Delta u_2$). Then, the combination of these two output signals, Δu_2 and Δu_3 with reference signal ($m_{2,0}$) is delivered to a low-pass filter to generate the most effective control signal, m_2.

3.5 Optimization algorithms

Here, the optimization procedures used in this work have been discussed. The aim of optimization is to solve the problem of finding the parameters that maximize or minimize a given real valued function. It is to be noted that the detailed discussion of these algorithms are not scope of this work, but the interested one may study in detail to the research [36, 40]. In this thesis, the applied optimization algorithms provide a scope to select optimal parameters that confirm the design of optimal damping controller.

3.5.1 Particle swarm optimization (PSO)

PSO is a novel population based meta-heuristic algorithm invented by Kennedy and Eberhart in 1995 [40]. PSO uses the social manners for instance, fish schooling and birds flocking to provide alternative solution to optimization problem characterized by non-linear in nature. The procedure PSO follows is about sharing individual knowledge of fishes or birds originated from group communication during the period of migration or food searching. However, it is very common that the finest path of food searching will not be known to all and once it is identified by one member, rest of the group follow that path.

In PSO, every individual person from the population is known as a particle and the entire population is named as swarm. The algorithm begins with an arbitrarily introduced population and moves in arbitrarily selected route. Each particle remembers the previous best records of its own and neighbors during the period of crossing in the searching space. Particles of a swarm educate better positions to one another as well as progressively alter their very own position and speed originated from the best position of whole particles. At whatever points every one of the particles have finished their development to another position, the subsequent stage starts. All particles in this manner will in general fly towards better positions over the searching procedure until the swarm go to an ideal estimation of the objective function. Consider a search space of N-dimensional shape at the starting (N denotes the number of particle that needs to be optimized) and x_i^0s are produced within the boundary limit $x_{min} < x_i^0 < x_{max}$ where x_{min} and x_{max} are denoted as lower and upper boundary limit of the search region. Current fitness value is calculated from the initial fitness of x_i^0. It is to be mentioned that minimum current fitness values are recoded as personal best $j_{ind,i}^0$ whereas the lowest value of personal best is termed as global best j_{best}^0. The position of particle corresponding to p_{best} and g_{best} is recoded as p_{best}^0 and g_{best}^0 respectively. In the event that x_i^t indicates the position vector of particle *i* in the N-dimensional search space at time step *t*, at that point the situation of every particle is modified time to time in the search space according to the following equations [40].

$$v_i^{t+1} = v_i^t + c_1(pbest_i^t - x_i^t) + c_2(gbest_i^t - x_i^t) \tag{3.9}$$

$$x_i^{t+1} = x_i^t + v_i^{t+1} \tag{3.10}$$

Where, $x_{min} < x_i^0 < x_{max}$ and v_i^t is the velocity vector of particle *i* that drives the advancement procedure and reflects both individual and social experience information from every one of the particles; x_{min} and x_{max} are the separate nearest and farthest points of boundary of the search space. Different steps of PSO algorithm are described below.

- Step 1: Define the problem space and set the boundaries.
- Step 2: Initialize an array of particles with random positions and velocities inside the problem space.
- Step 3: Check if the current position is inside the problem space or not. If not, adjust the positions so as to be inside the problem space.

- Step 4: Evaluate the fitness of each particle.
- Step 5: Compare the current fitness value with the particle's previous best value p_{best}. If the current fitness value is better, assign the current value to p_{best} update the current coordinates.
- Step 6: Determine the current global minimum among the molecule's best position (g_{best}).
- Step 7: If the current global minimum is superior to g_{best}, employ the present value to g_{best} and update the current global best positions.
- Step 8: Update the velocity according to the equation (3.9).
- Step 9: Move every particle to the new position according to the equation (3.10) and go back to Step 3.
- Step 10: Repeat Step 3 to Step 9 until the stopping criteria is fulfilled.

3.5.2 Differential evolution (DE) algorithm

DE is one of the progressive algorithms which have striking properties of resolving optimization complications. The elementary DE algorithm was first suggested by Storn and Price in 1997 [25]. The main steps of DE algorithm are initialization of a group, mutation, recombination and selection. Various steps related to DE algorithm are discussed below:

- Step 1: This step is called initialization; an arbitrary set of probable solution for each component is generated within the search space. If an objective function having D real parameters is to be adjusted for a primary population size NP, the parameters vector includes the following form.

$$X_{i,G} = [x_{1,i,G}, x_{2,i,G}, \dots \dots \dots \dots \dots x_{D,i,G}] \quad (3.11)$$

  Where, i = 1, 2, ... … … NP and G is the generation number.

  The maximum and minimum limit for each parameter, $x_j^L \leq x_{j,i,1} \leq x_j^U$.

  The arbitrary parameters in each generation should lie within the interval, $[x_j^L, x_j^U]$.

- Step 2: Three target vectors $x_{r1,G}$, $x_{r2,G}$ and $x_{r3,G}$ are arbitrarily nominated from a specified parameter vector $X_{i,G}$ for the mutation phase keeping in notice that the keys r_1, r_2, r_3 and i are different. These three vectors with mutation factor M_F are used to produce the donor vector as below [59].

$$V_{i,G+1} = x_{r1,G} + M_F(x_{r2,G} - x_{r3,G}) \quad (3.12)$$

- **Step 3:** In this recombination step, trial vector denoted by $V_{j,i,G+1}$ is generated and the trial vector gets updated by donor vector which have probability of C_R.

$$V_{j,i,G+1} = \begin{cases} V_{j,i,G+1}, & if\ rand_{j,i} \leq C_R\ or\ j = I_{rand} \\ V_{j,i,G}, & if\ rand_{j,i} \leq C_R\ or\ j \neq I_{rand} \end{cases} \quad (3.13)$$

Where,

$rand_{j,i}$ is a arbitrary number having the range within [0, 1]

I_{rand} is a random integer which is taken from [1, 2, …….., D].

- Step 4: In the selection step, an evaluation is made between target vector and trial vector and ones with the best value is chosen and others sent to the generation for repeating.

$$x_{i,G+1} = V_{i,G+1} \quad \text{if } j(V_{i,G+1}) \leq j(x_{i,G}) \quad (3.14)$$
$$= x_{i,G} \quad \text{otherwise}$$

The mutation, recombination and selection steps proceed until a pre-indicated stopping is achieved.

3.6 Objective functions

To select the most effective controller parameters that enhance most the power system transient performance, eigenvalue based objective functions are considered. The objective function is subjected to inequality constraints which are the limits of each controller gain K and time constants T_1 & T_2. In this work, the following two eigenvalue based objective functions have been proposed for the controller design problem [26].

$$J_1 = \sum_{i=1}^{n}(\sigma_i - \sigma_0)^2 \quad (3.15)$$

$$J_2 = \sum_{i=1}^{n}(\xi_0 - \xi_i)^2 \quad (3.16)$$

$$J = -(J_1 + W_F * J_2) \quad (3.17)$$

Where,

σ_i is the real part of i_{th} eigenvalues,

σ_0 is the estimation of the real part of eigenvalues,

ξ_i is the real part of i_{th} damping proportions,

ξ_0 is the estimations of damping proportions,

W_F is the weighting factor which is taken 0.1.

The optimization of J_1 will guarantee that the real part of the eigenvalues is lying close to the desired position and the optimization of J_2 will ensure that the adequate damping has been introduced to the system. In this way, minimization of J will guarantee that both J_1 and J_2 destinations are satisfied simultaneously while an optimization of controller gains is acquired. Therefore, in order to depict the optimization problem constraints of the parameter can be represented as follows.

$$K_{min} \leq K \leq K_{max}$$

$$T_{1min} \leq T_1 \leq T_{1max}$$

$$T_{2min} \leq T_2 \leq T_{2max}$$

3.7 Controller Parameter Optimization

The main goal of employing optimization algorithm is to select the optimal parameters of controller among the different options to operate system in optimal conditions. In proposed damping controller design, two different optimizers such as PSO and DE are considered to tune the controller parameters (K, T_1, T_2) for enhancement of damping ratio; since improper tuning may lead to sub-optimal outcomes. However, since the optimization method for these algorithms are different, they have some similar as well as dissimilar parameters that need to be defined. In order to obtain best result, it is taken that the maximum population size is 100, the maximum number of iteration is 100, and the number of runs is 30 which similar parameters are for both PSO and DE; whereas, dissimilar parameters for PSO are cognitive accelerating coefficient is 2, social accelerating coefficient is 1.5 and for DE are mutation factor is 0.8 & crossover probability is 0.2 are considered for this work. After defining the parameters for these optimization algorithms, to keep the search space within practically feasible limits, the controller parameters are bounded by defining upper and lower limits as in Table 3.2. Further, in order to perform optimization using these algorithms, an eigenvalue based objective function is to be considered [26], whose minimization will ensure the desired optimal control parameters. It is to be noted that, eigenvalue based objective function exhibits better performance than time domain based objective function in terms of computational time [28].

Table 3.2: Boundary and optimized value of controller parameters for different load

Controller Parameter	Boundary Value		Optimized Value					
			PSO			DE		
	Lower Limit	Upper Limit	Nominal Load	Light Load	Heavy Load	Nominal Load	Light Load	Heavy Load
k_p	-50	50	-18.6896	-33.9278	-13.0922	-18.2420	-38.4458	-12.4281
k_i	-50	50	-3.7687	-19.2741	-5.9292	-1.6058	-16.4578	-4.2617
T_1	0.01	10	4.7368	5.0190	6.9370	7.0836	10.0000	5.6879
T_2	0.01	10	3.2437	1.9291	4.1982	4.6119	5.0562	3.0593
k_{dc}	0.01	50	28.0755	31.8611	25.8302	26.9459	36.7072	22.9660
T_w	0.01	10	4.2269	6.4444	8.0085	4.4686	2.7354	5.4816

Moreover, to find the most excellent optimization algorithm among these two, their performances are compared in terms of elapsed time and best fitness value obtained from multiple runs (30). Finally, two different statistical analyses have been performed to find out significant differences among these algorithms, which will be discussed in next section.

3.8 Time domain analysis

Time domain simulation lacks some features such as relevant information regarding various weak modes, the overriding states variable associated with weak modes and response of those modes to parameter variation and other details. Hence, for small signal stability analysis it is suggested to perform both eigenvalue and time domain analyses, where it is utilized as reciprocal answers for helping one another and confirm the outcomes. In time domain analysis, mode is perturbed and the behavior of state variable is calculated by solving differential equations using some numerical integration techniques with the known initial values [20, 21, 22]. In this case, the initial values are the initial operating point. Both eigenvalue and time domain analyses have been used in this research. The dynamic characteristics such as peak overshoot, peak undershoot and settling time of the state can be realized easily from time domain analysis. When a system is subjected to small disturbance it experiences transient condition means oscillation which may be sustained or decayed. The certain behavior of the system relies on the parameters of the system.

From the time domain simulation it is observed that, dynamic responses are started at the instant of disturbance and oscillation sustains for a specific period until adequate damping is provided.

3.9 Non-parametric statistical test

In this work, the non-parametric statistical tests such as Kolmogorov-Smirnov test is utilized in order to identify the presence of significant non-uniformity among above mentioned optimizers. For this purpose, each of the optimizers have been run several times (30) to obtain corresponding fitness values and to supply these fitness values as input to IBM SPSS (version 23) software. In case of Kolmogorov-Smirnov test, to identify the nature of data-set distribution, considered two hypotheses such as null hypothesis, H_0 accepts the data set agreed with normal distribution whereas, alternate hypothesis, H_1 rejects the decision of H_0 with 5% significance level [23]. For Paired sample *t*-test, to justify statistically significant correlations among data-set, considered two hypotheses based on Asymp. Sig. 2-tailed value (p-value), such as null hypothesis, H_0 accepts if the data sets are correlated and alternate hypothesis, H_1 admits if the data sets are different with a significant level of 0.05.

3.10 Parameters of IPFC equipped SMIB system

To perform the analysis of the system performance, the following parameter's values are utilized for this research work [27].

Table 3.3: Parameters of IPFC equipped SMIB system

Item	**Parameter's Values**
Generator	$x_d = 1.80\ \text{pu}, x_q = 0.7\ \text{pu}, x'_d = 0.55\ \text{pu}, D = 0\ \text{pu},$ $M = 8\ \text{MJ/MVA}, \omega = 100\pi, T_{d0}' = 2.19\ \text{pu}$
Transformer	$x_t = 0.1\ \text{pu}$
Transmission line	$x_{l1} = 0.9\ \text{pu}, x_{l2} = 0.9\ \text{pu}$
Converter transformers	$x_{t1} = 0.1\ \text{pu}, x_{t2} = 0.1\ \text{pu}$
Exciter	$T_A = 0.01\text{sec}, K_A = 50$
DC link	$V_{dc} = 2\ \text{pu}, C_{dc} = 1\ \text{pu}$
Nominal Voltage	$V_s = 1\ \text{pu}$

Chapter 4
Analysis of IPFC

In this chapter, the controllability test analysis in open loop condition is described in section 4.1. Section 4.2 illustrates eigenvalue analysis in close-loop condition. The time domain simulation results such as without controller at open loop condition, with controller and with two optimizers (PSO, DE) at closed loop condition on nominal, light & heavy load conditions with various disturbances are shown in section 4.3. Section 4.4 the critical analysis of the simulation results are discussed. Section 4.5 explains the quantitative analysis between these optimizers. In the end of this chapter, the non-parametric statistical analysis result is explained in section 4.6.

4.1 Controllability test analysis in open loop

The controllability test analysis is performed by using the state matrices A and B in open loop condition without controller. The controllability matrix (5x20) is obtained from the matrices A (5x5) and B (5x4). A system is controllable if uncontrollability is equal to zero, otherwise the system is not controllable. The uncontrollability defined as the difference between the length (longest dimension) of state matrix, A and the rank of controllability matrix of a system, mathematically it can be expressed as the following.

Uncontrollability = n – r

= 5 – 5= 0

Here, n = longest dimension of state matrix, A (5x5) = 5

r = rank of controllability matrix (5x20) of the system= 5

Therefore, it is observed that uncontrollability of the system is equal to zero, the system is controllable.

4.2 Eigenvalue analysis in close-loop

Here, eigenvalue analysis is performed for lead-lag controller based close-loop system, where PSO and DE optimizers have been employed to tune these controllers. In open-loop system, it is observed that the positive real values of 0.3947 and0.0203associated with (δ, ω) and V_{dc} are

existed that indicate the system unstable. But after adopting lead-lag controller integrated two optimizers in close-loop system, the positive real values are shifted into negative real values of -5.2585 & -0.2532 for PSO and -5.3620 & -0.2194 for DE associated with same states respectively whose are shown in Table 4.1.The negative real values indicate the system stable.

Table 4.1: Eigenvalues with Lead-Lag integrated controller

Associated State	**Close loop eigenvalues**		**Open loop eigenvalues**
	PSO	**DE**	
E_{fd}	-99.4240	-99.4240	-91.6101
$E_q^{'}$	-0.6526	-0.6715	-10.1923
δ, ω	-5.2585$\pm$ 0.0290i	-5.3620 $\pm$ 0.0005i	0.3947 $\pm j$6.5774
V_{dc}	-0.2532	-0.2194 + 0.0085i	0.0203
$m_2, \Delta u_3$	-7.3574$\pm$ 7.7286i	-7.3160 $\pm$ 7.7368i	- - - - -
Δu_2	-0.2978	-0.0965	- - - - -
Δu_1	-0.2320	-0.2194 - 0.0085i	- - - - -

Therefore, it has been observed clearly that after applying controller equipped optimizers the unstable system has become stable.

4.3 Time domain simulation

To perform time domain simulation, a small perturbation is introduced to study system by applying a sudden mechanical input changes after 0.1 second of the starting of the simulation with a step change of 0.1 p.u. in order to analyze the performance of the tuned controllers by observing the nature of speed deviation in terms of overshoot, undershoot, and settling time. In this work, the time domain simulation is performed for nominal load (P_e = 1.0 p.u., Q = 0.268 p.u.), light load (P_e = 0.3 p.u., Q = 0.08 p.u.), and heavy load (P_e = 1.1 p.u., Q = 0.4 p.u.) to validate the effectiveness of our tuned controllers, since consideration of such loading conditions are more practical and hence, are widely implemented in the literature [29]. Now, considering these loading conditions with various disturbances, the results of time domain simulation for tuned lead lag controller have been depicted in Fig. 4.1 to Fig. 4.15 respectively.

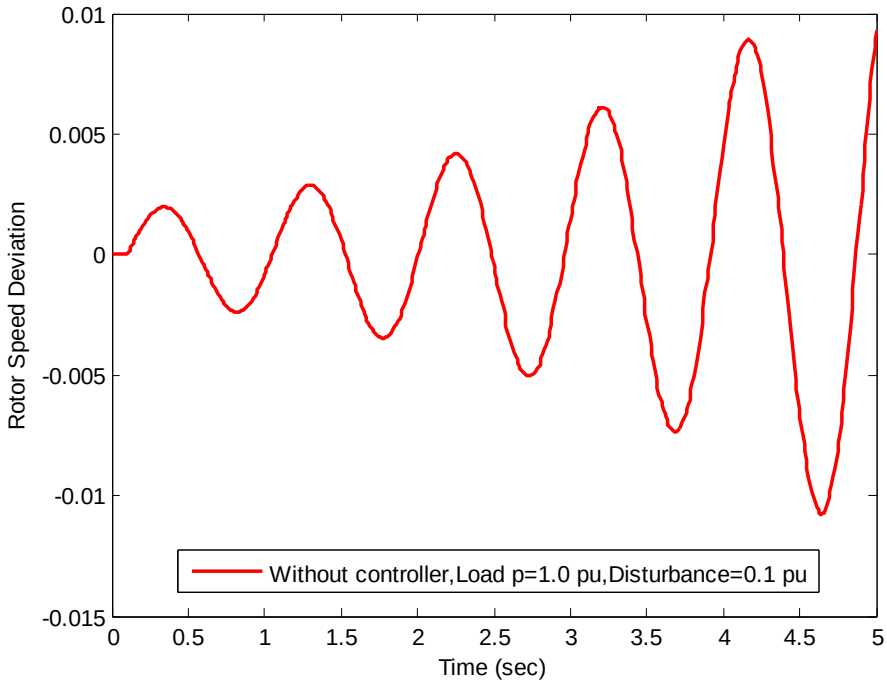

Figure 4.1: Time-domain simulation of rotor speed deviation without controller for nominal load with disturbance 0.1 pu

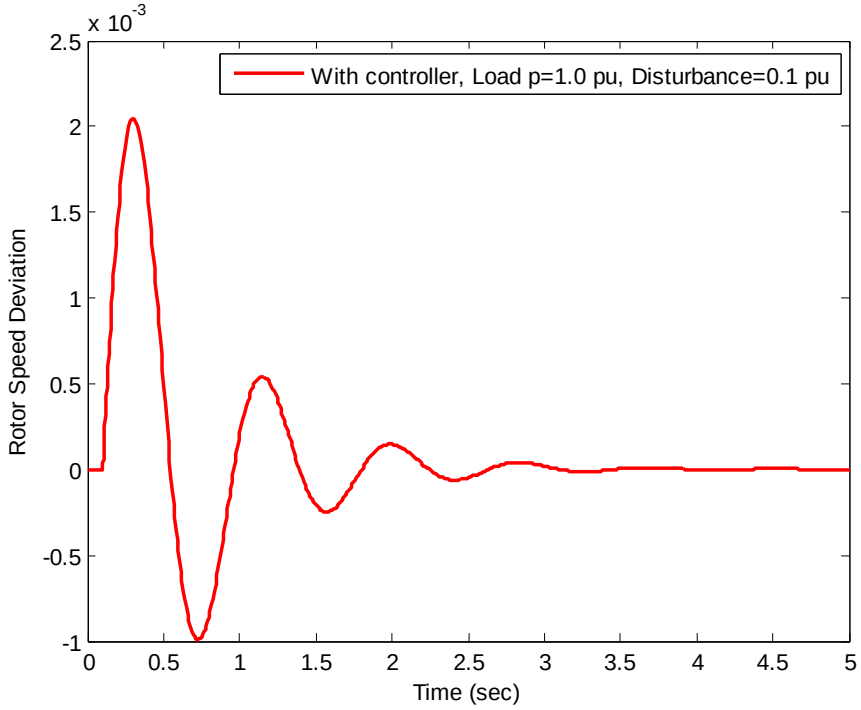

Figure 4.2: Time-domain simulation of rotor speed deviation with controller for nominal load with disturbance 0.1 pu

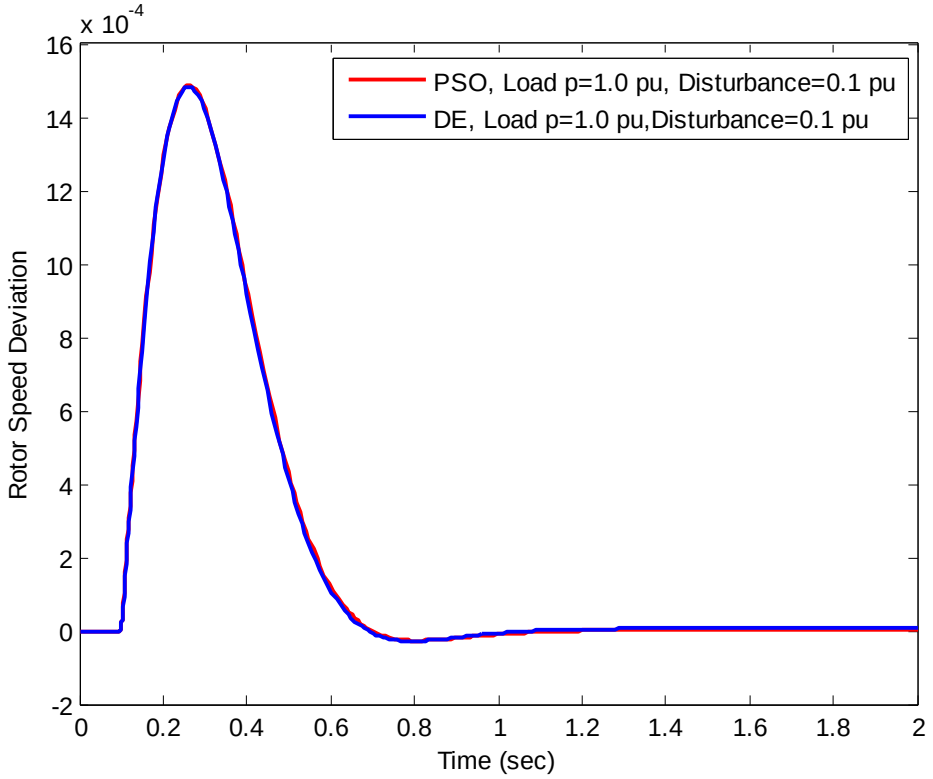

Figure 4.3: Time-domain simulation of rotor speed deviation with PSO & DE optimizers for nominal load with disturbance 0.1 pu

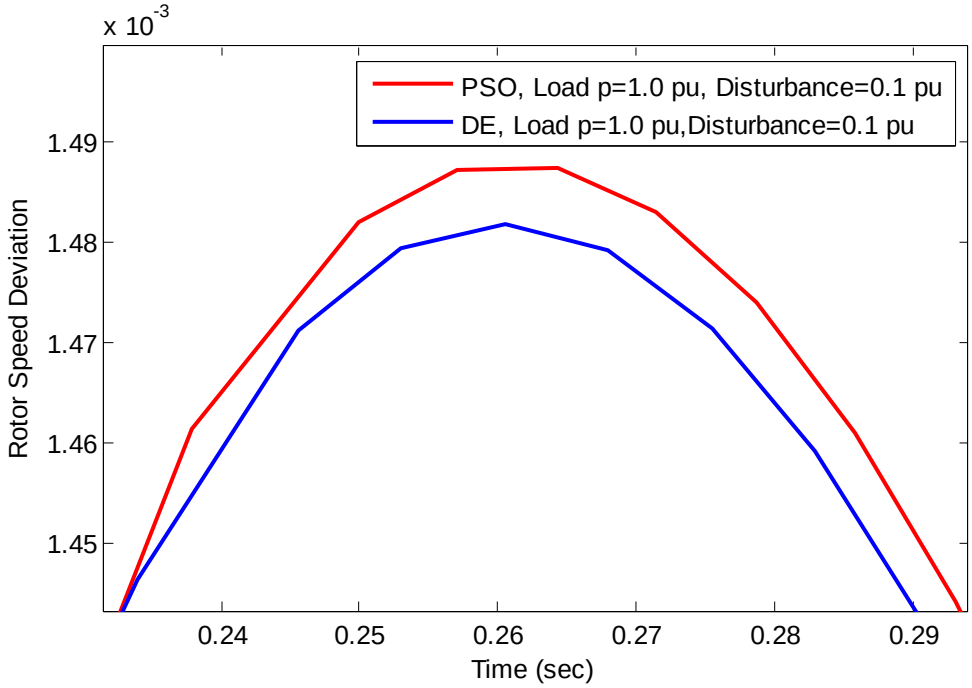

Figure 4.4: Zoom view of overshoot for Fig.4.3

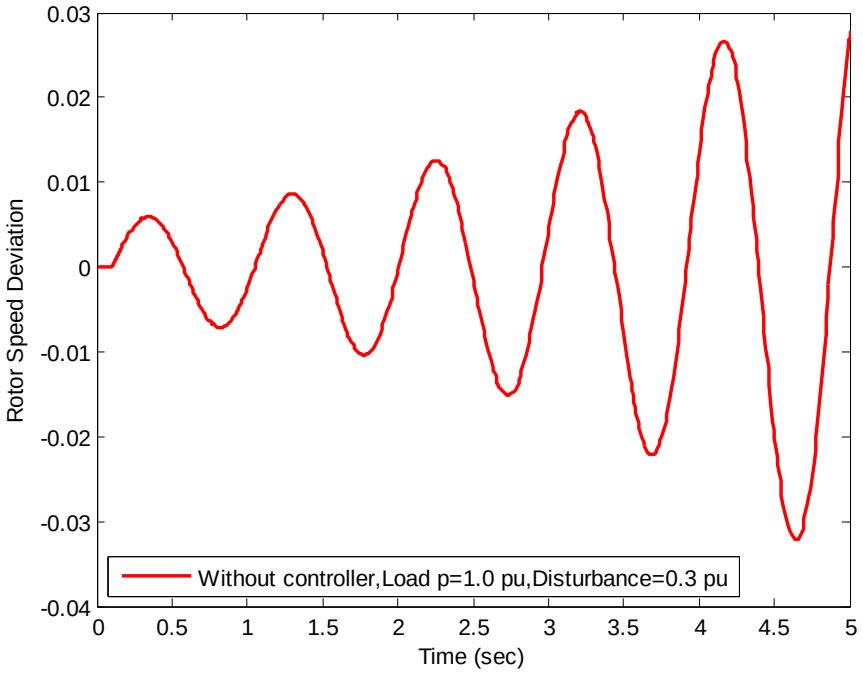

Figure 4.5: Time-domain simulation of rotor speed deviation without controller for nominal load with disturbance 0.3 pu

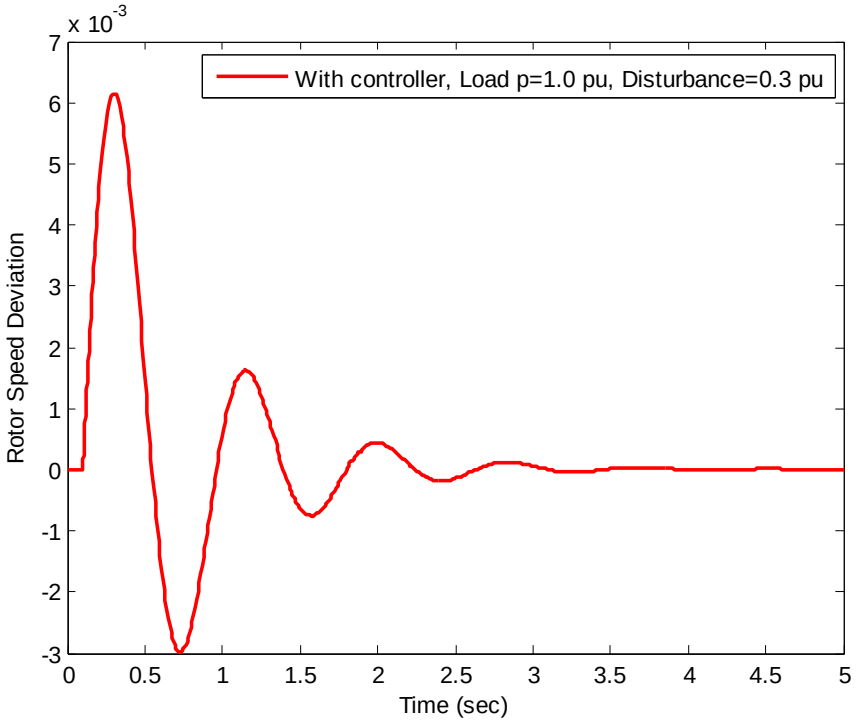

Figure 4.6: Time-domain simulation of rotor speed deviation with controller for nominal load with disturbance 0.3 pu

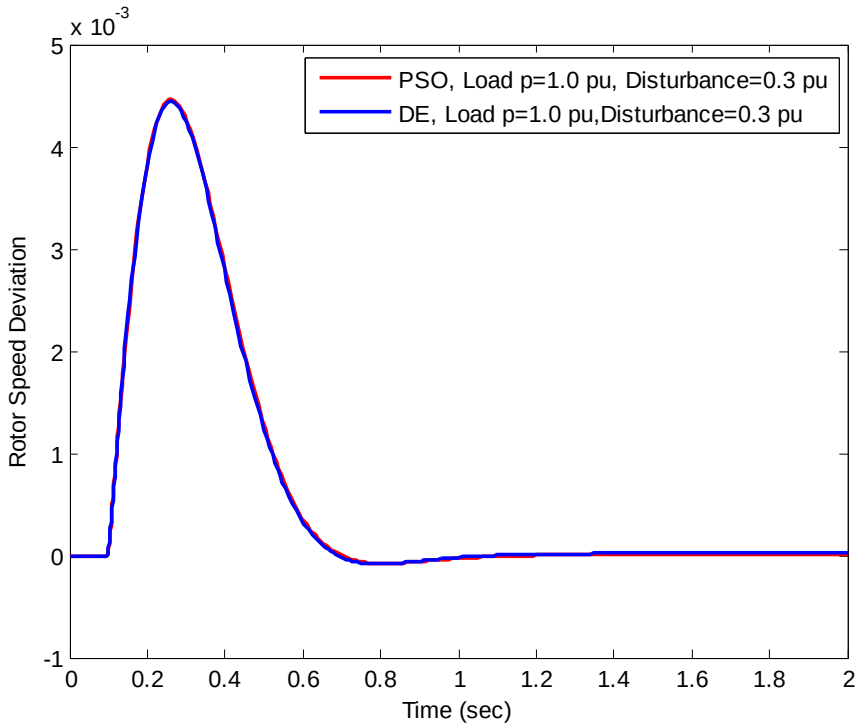

Figure 4.7: Time-domain simulation of rotor speed deviation with PSO & DE optimizers for nominal load with disturbance 0.3 pu

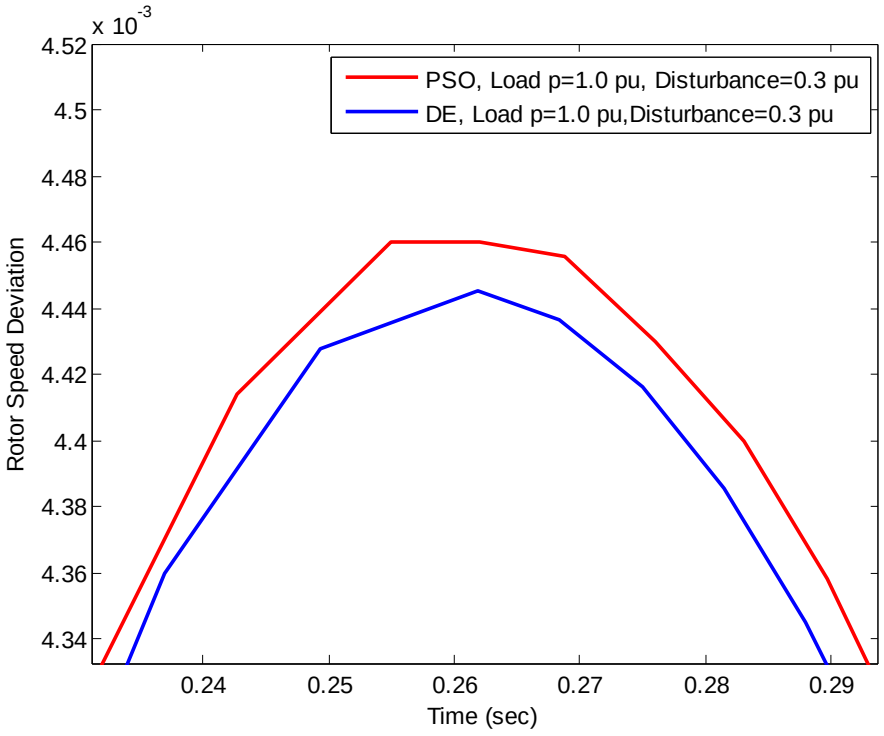

Figure 4.8: Zoom view of overshoot for Fig.4.7

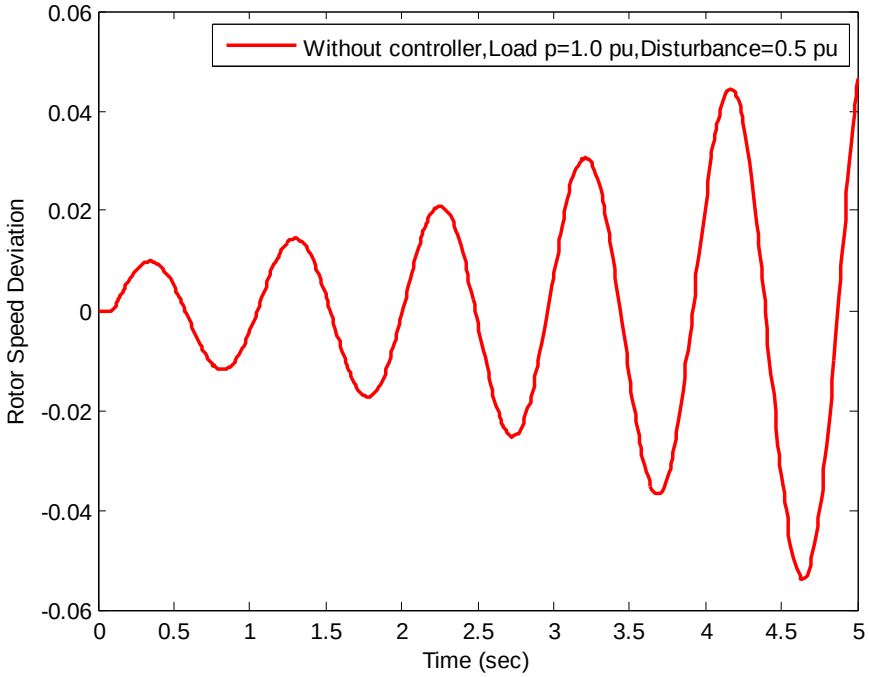

Figure 4.9: Time-domain simulation of rotor speed deviation without controller for nominal load with disturbance 0.5 pu

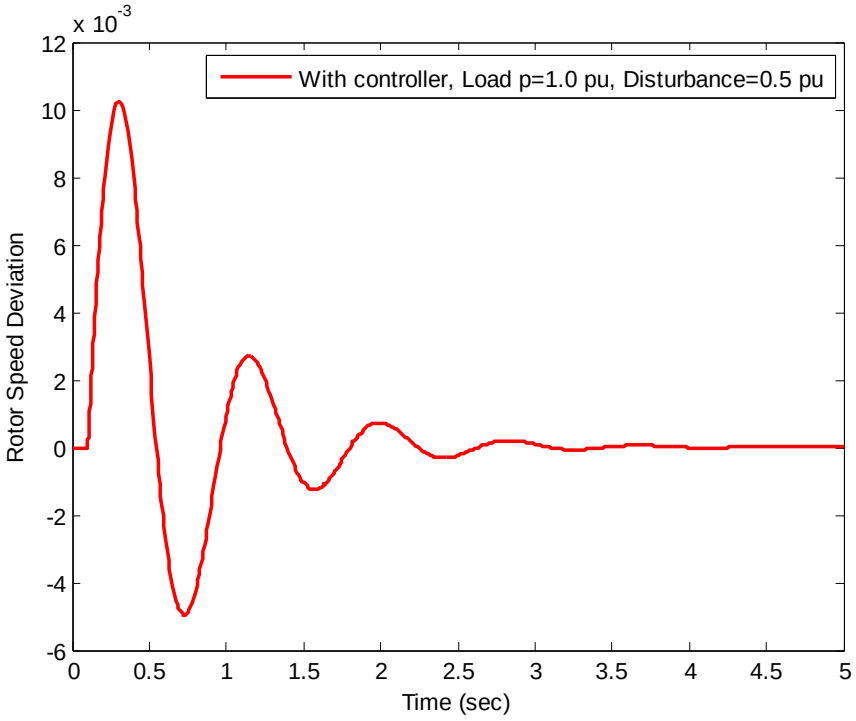

Figure 4.10: Time-domain simulation of rotor speed deviation with controller for nominal load with disturbance 0.5 pu

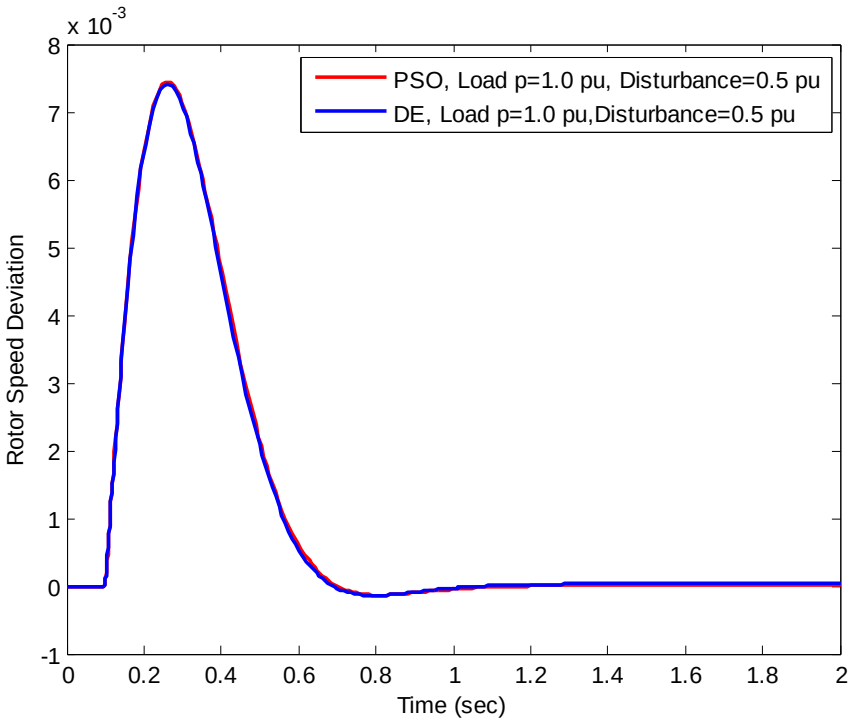

Figure 4.11: Time-domain simulation of rotor speed deviation with PSO & DE optimizers for nominal load with disturbance 0.5 pu

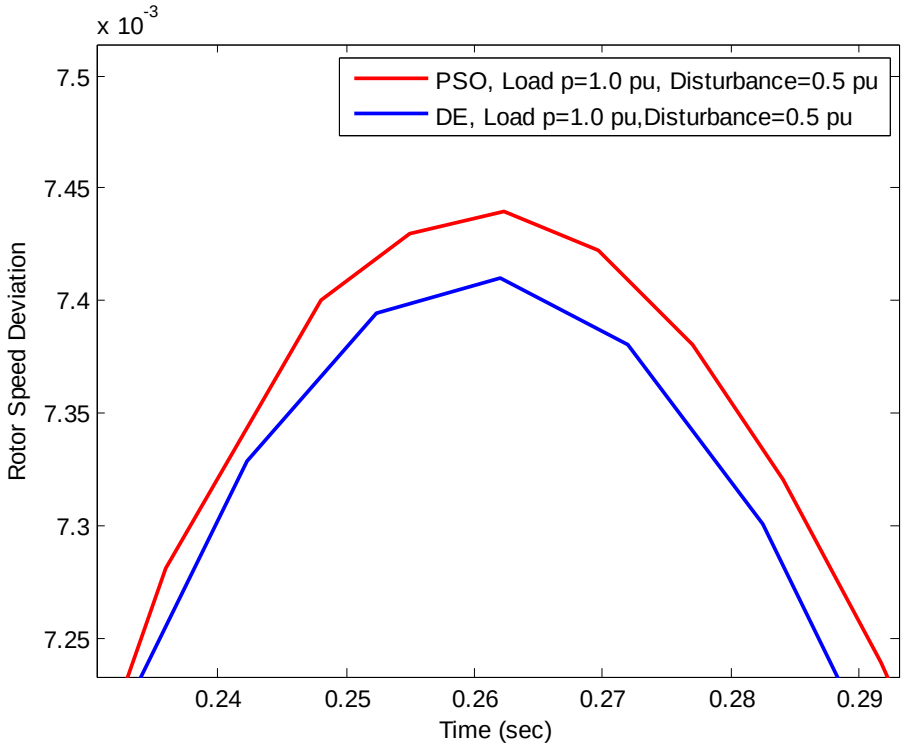

Figure 4.12: Zoom view of overshoot for Fig.4.11

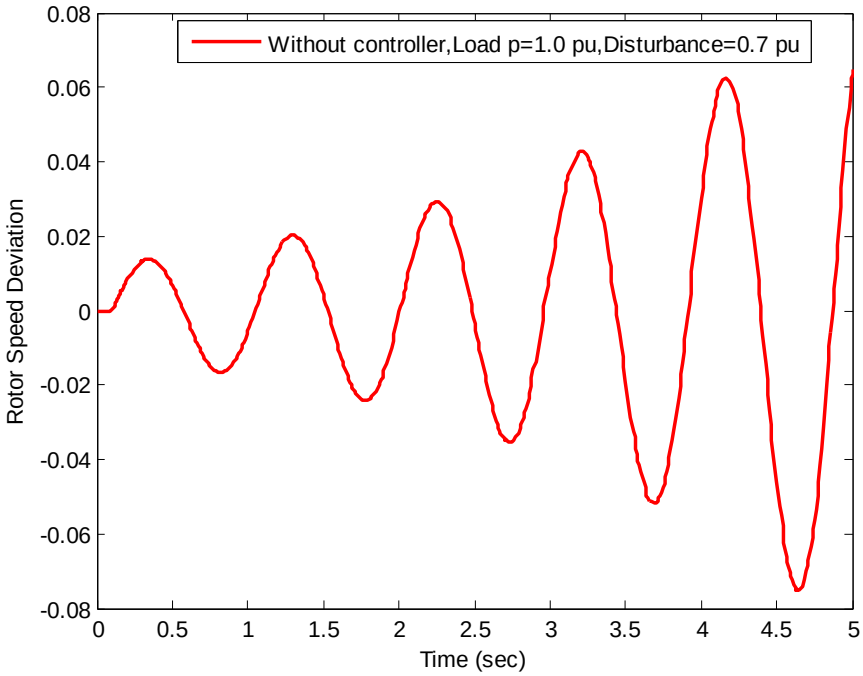

Figure 4.13: Time-domain simulation of rotor speed deviation without controller for nominal load with disturbance 0.7 pu

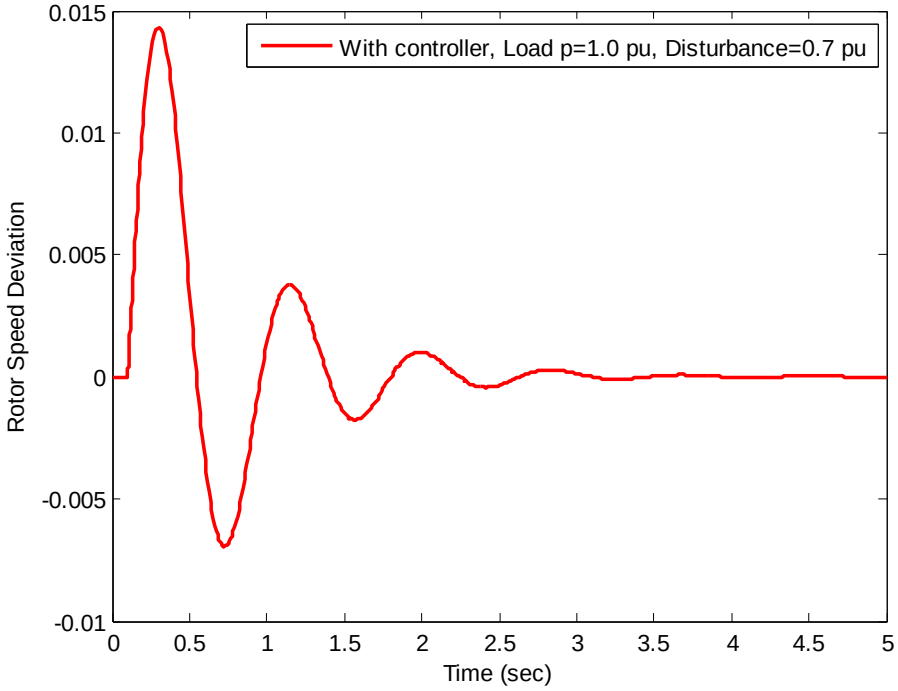

Figure 4.14: Time-domain simulation of rotor speed deviation with controller for nominal load with disturbance 0.7 pu

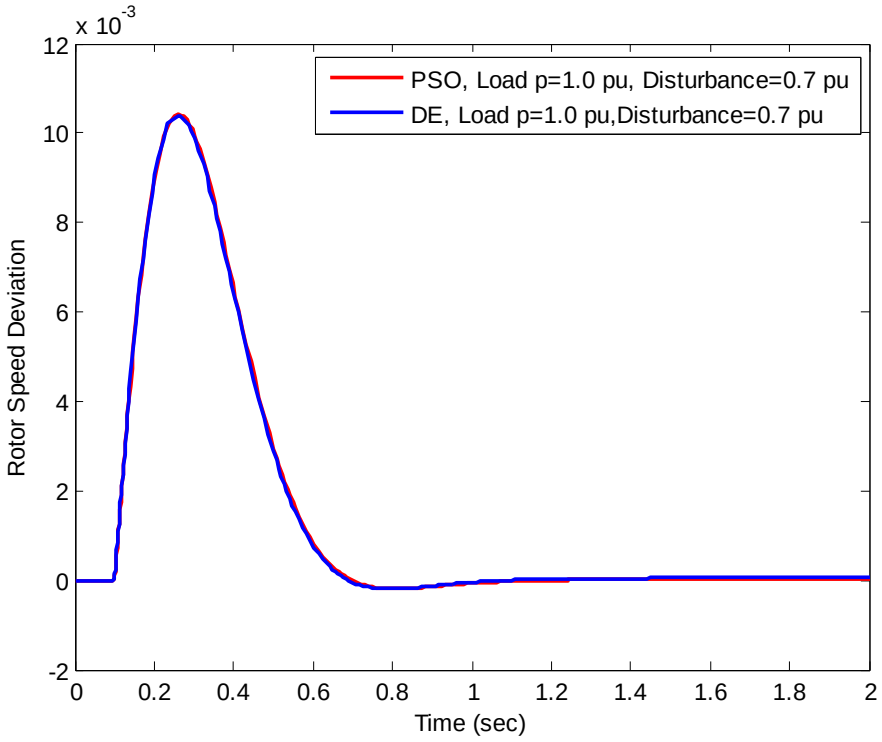

Figure 4.15: Time-domain simulation of rotor speed deviation with PSO & DE optimizers for nominal load with disturbance 0.7 pu

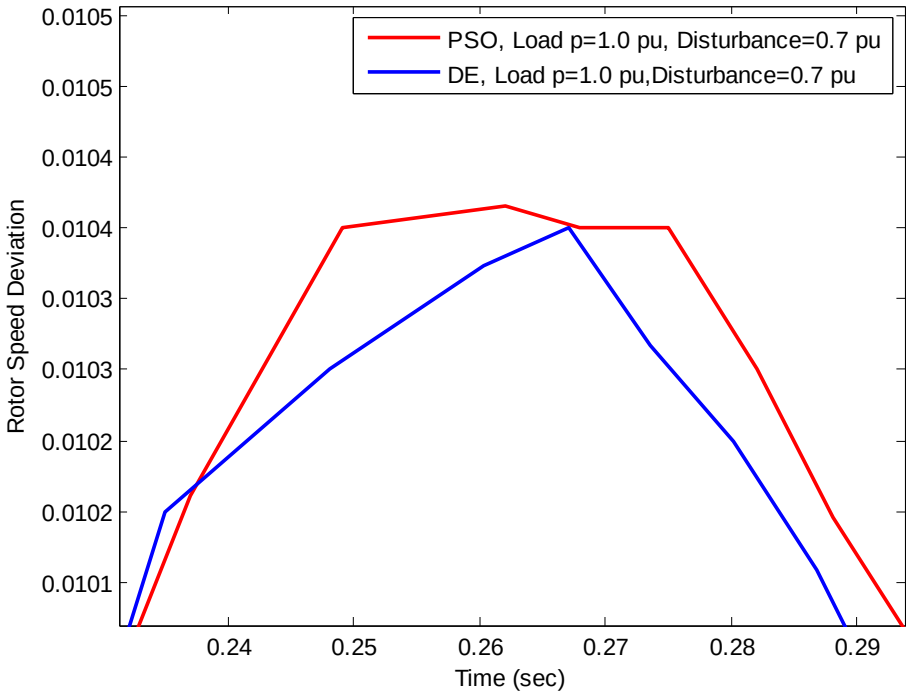

Figure 4.16: Zoom view of overshoot for Fig.4.15

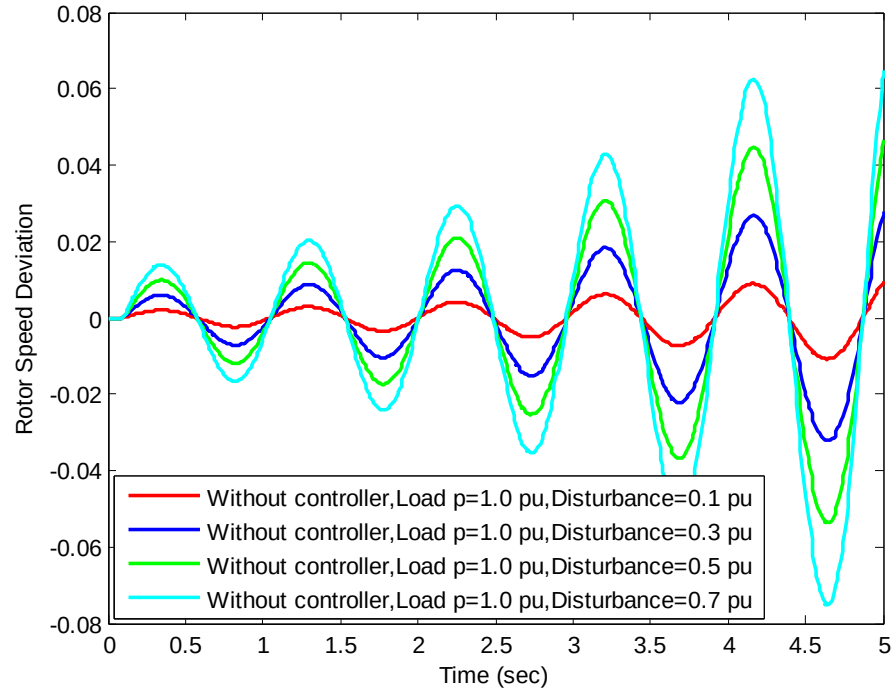

Figure 4.17: Time-domain simulation of rotor speed deviation for nominal load without controller for comparison of different disturbances

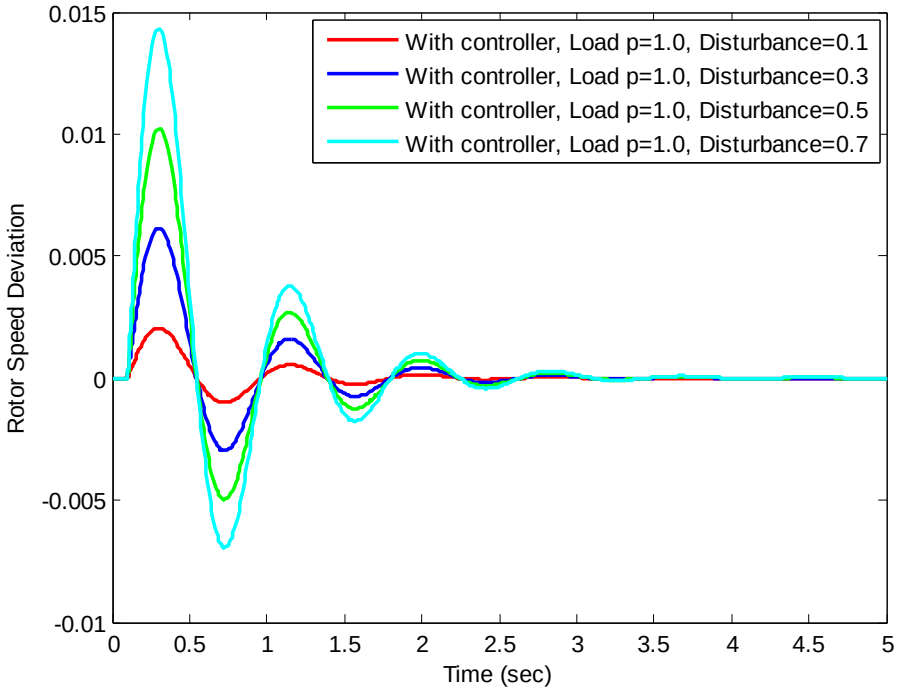

Figure 4.18: Time-domain simulation of rotor speed deviation for nominal load with controller for comparison of different disturbances

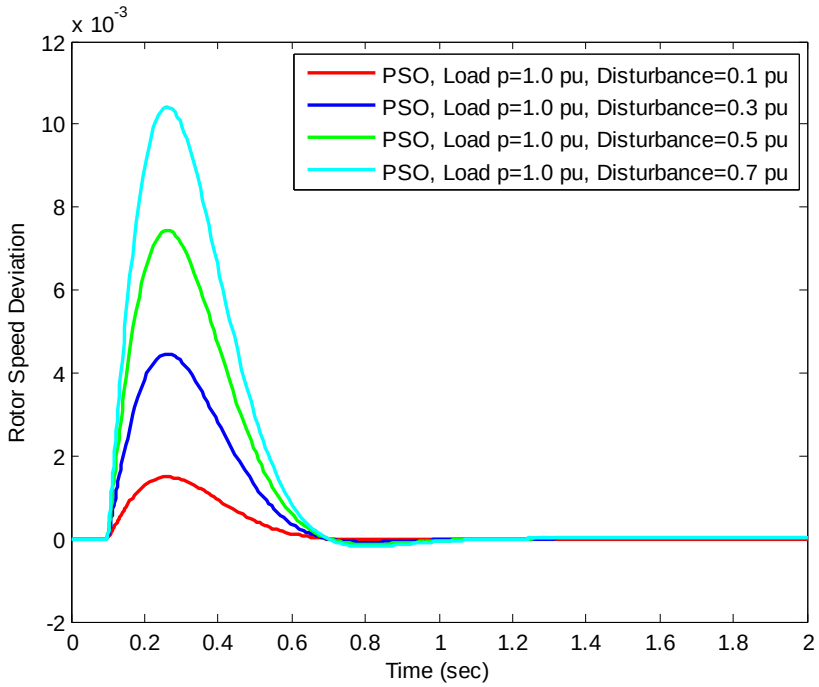

Figure 4.19: Time-domain simulation of rotor speed deviation for nominal load with PSO optimizer for comparison of different disturbances

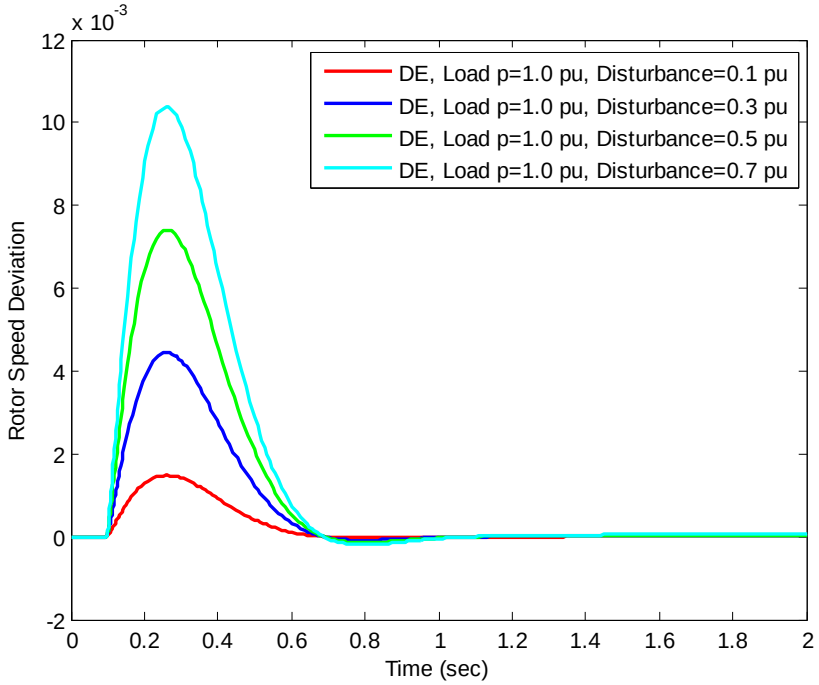

(d)

Figure 4.20: Time-domain simulation of rotor speed deviation for nominal load with DE optimizer for comparison of different disturbances

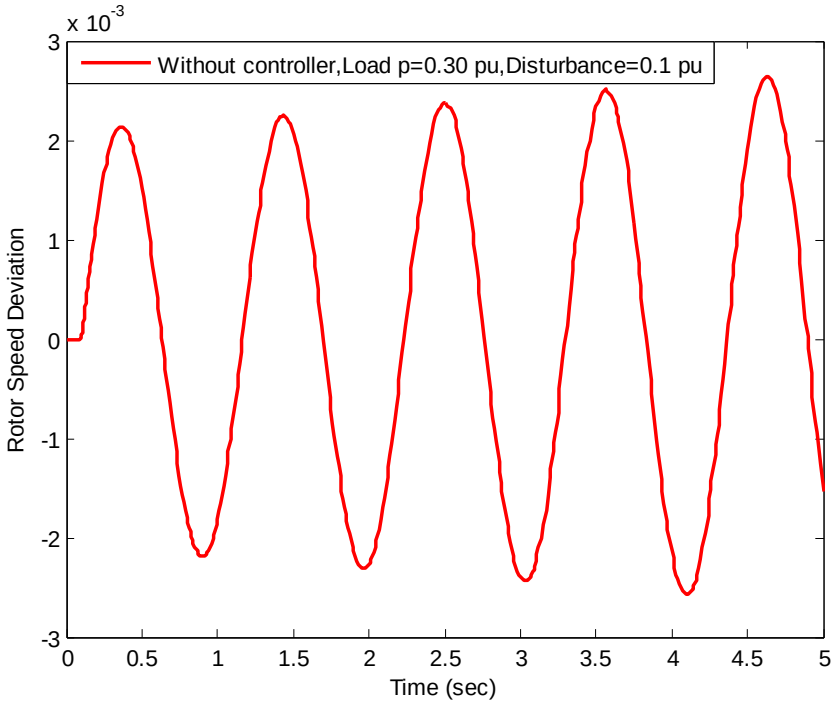

Figure 4.21: Time-domain simulation of rotor speed deviation without controller for light load with disturbance 0.1 pu

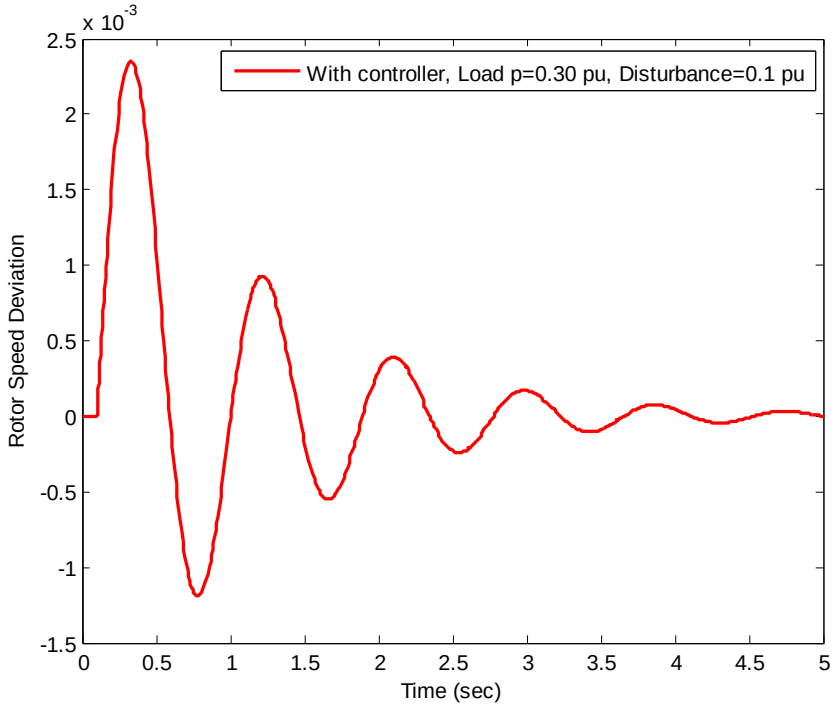

Figure 4.22: Time-domain simulation of rotor speed deviation with controller for light load with disturbance 0.1 pu

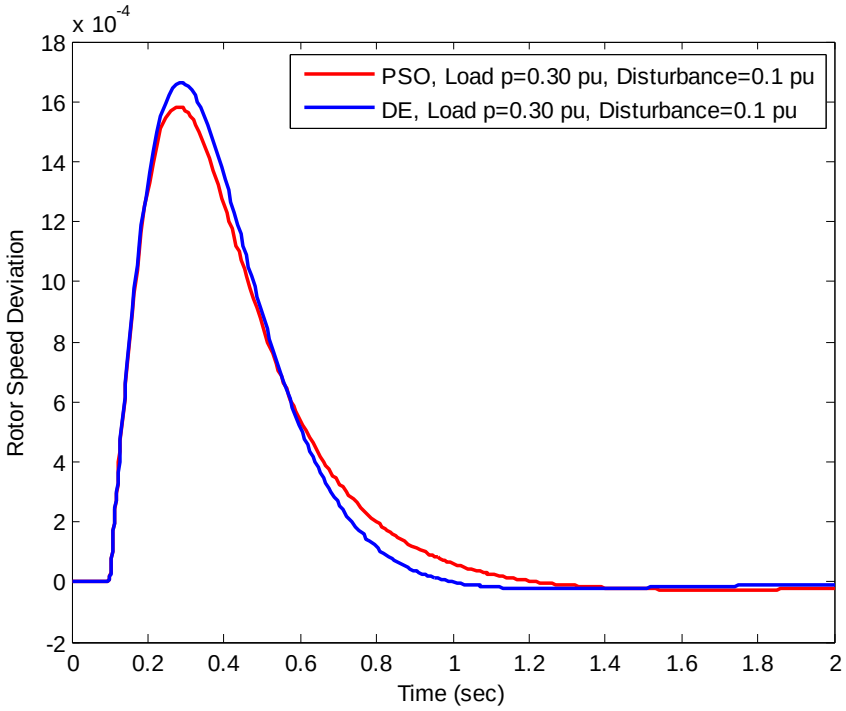

Figure 4.23: Time-domain simulation of rotor speed deviation with PSO & DE optimizers for light load with disturbance 0.1 pu

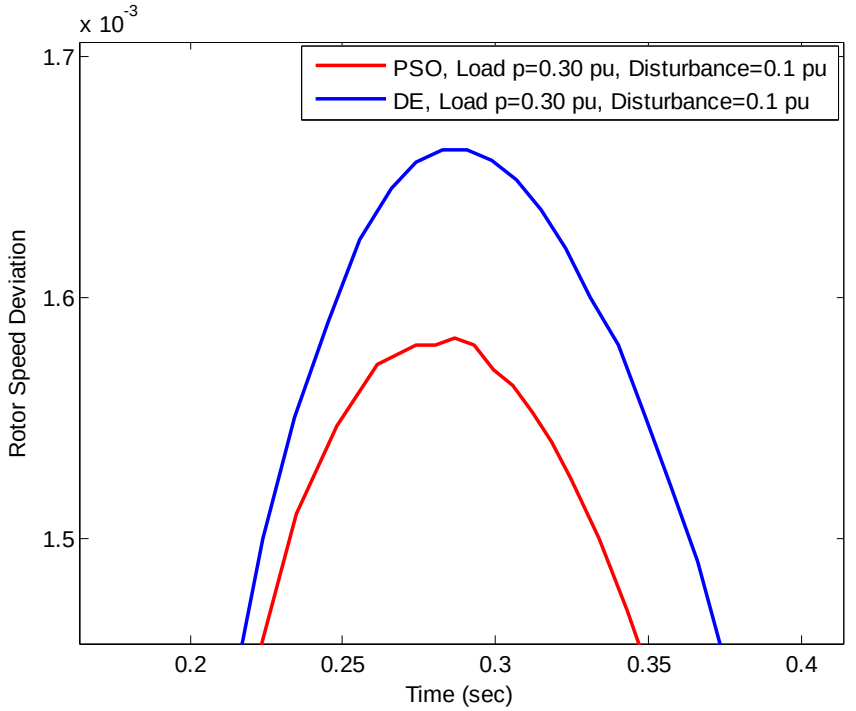

Figure 4.24: Zoom view of overshoot for Fig.4.23

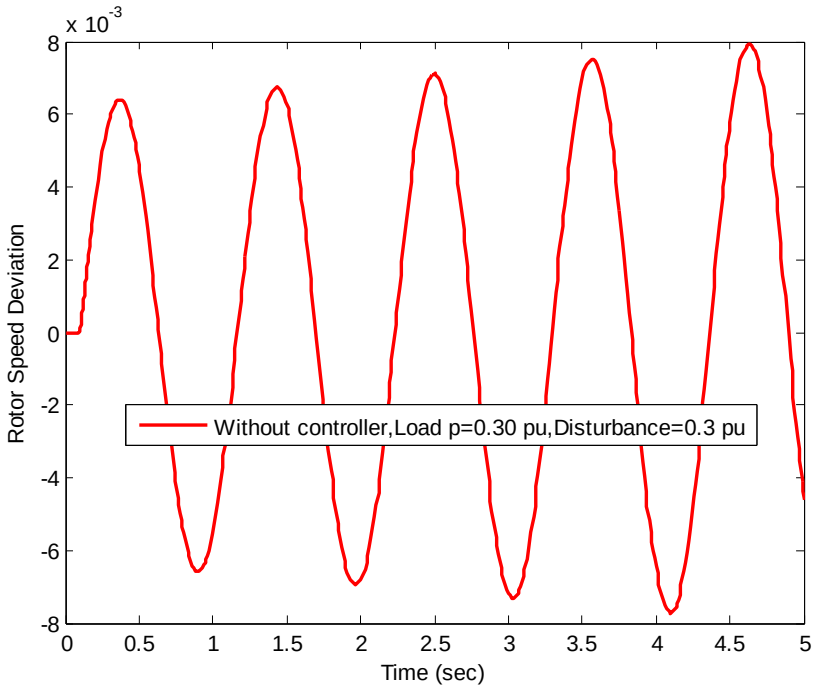

Figure 4.25: Time-domain simulation of rotor speed deviation without controller for light load with disturbance 0.3 pu

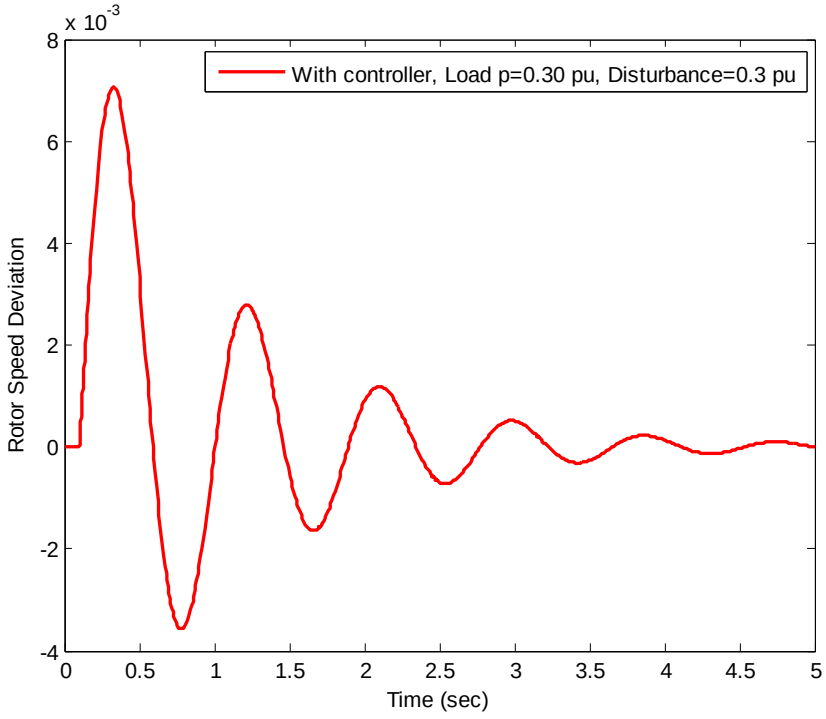

Figure 4.26: Time-domain simulation of rotor speed deviation with controller for light load with disturbance 0.3 pu

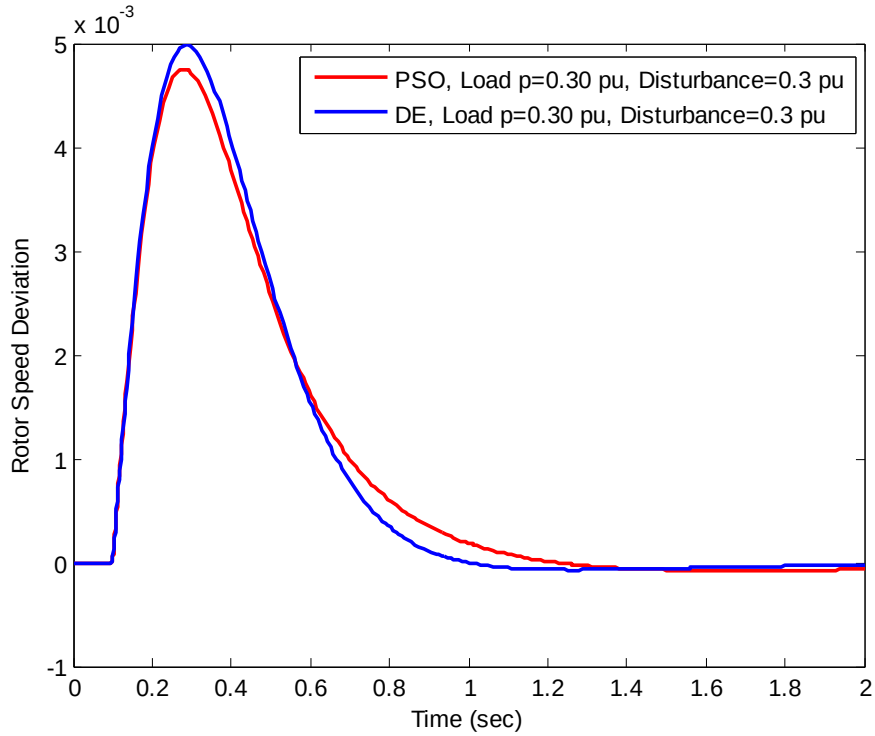

Figure 4.27: Time-domain simulation of rotor speed deviation with PSO & DE optimizers for light load with disturbance 0.3 pu

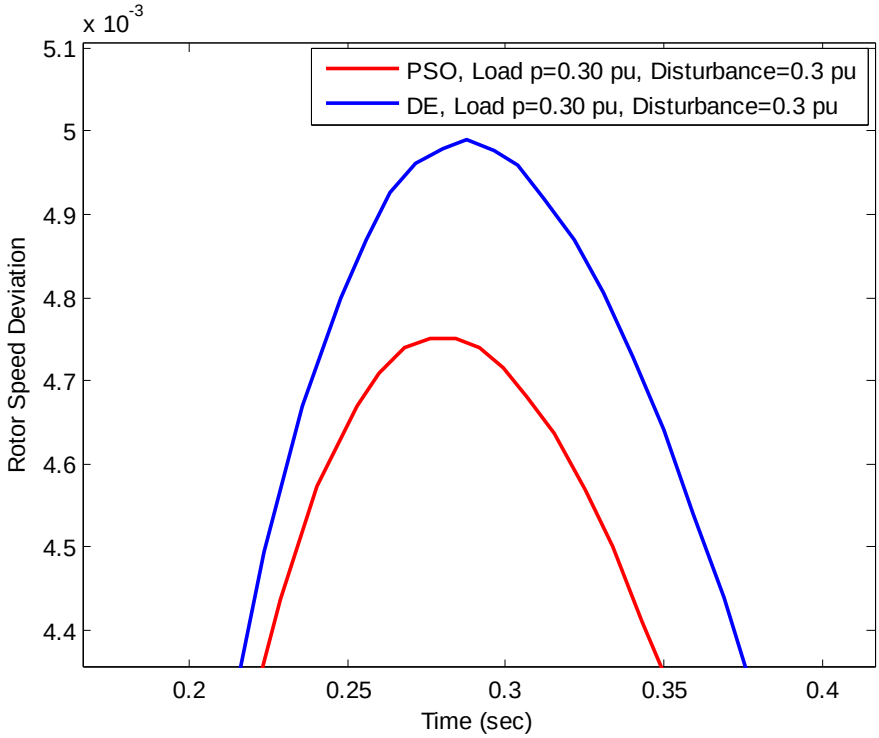

Figure 4.28: Zoom view of overshoot for Fig.4.27

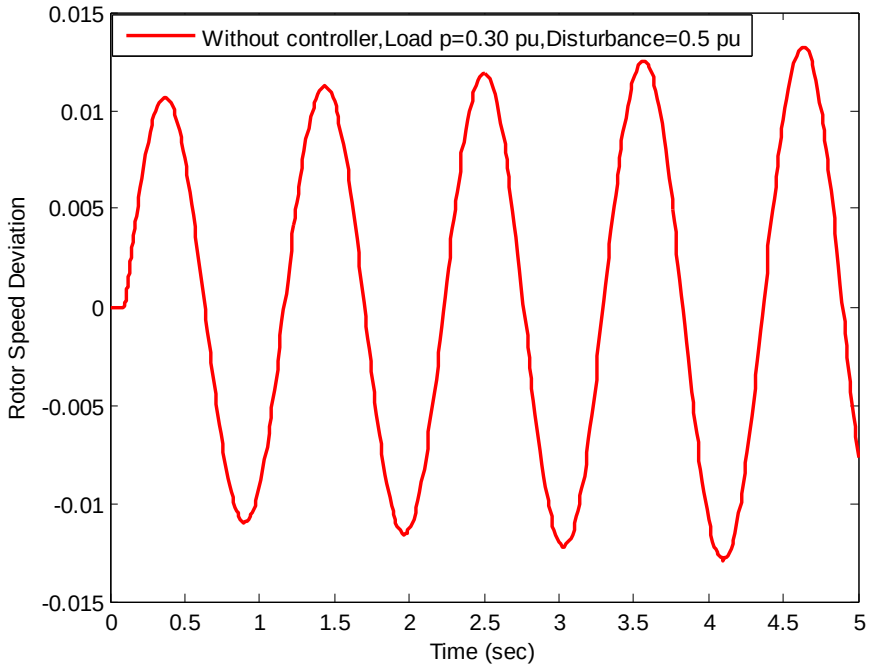

Figure 4.29: Time-domain simulation of rotor speed deviation without controller for light load with disturbance 0.5 pu

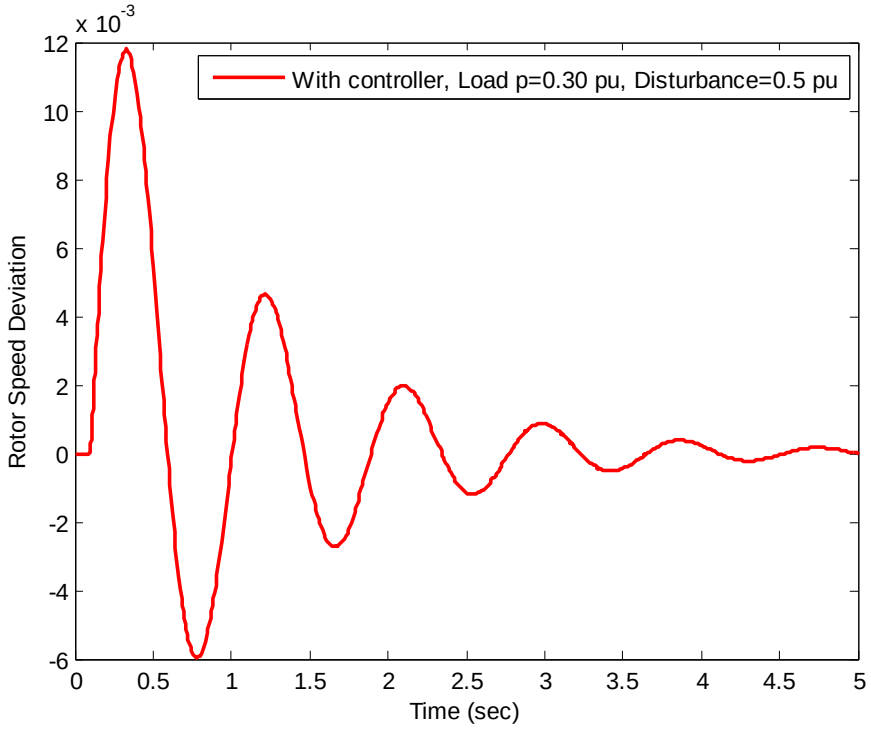

Figure 4.30: Time-domain simulation of rotor speed deviation with controller for light load with disturbance 0.5 pu

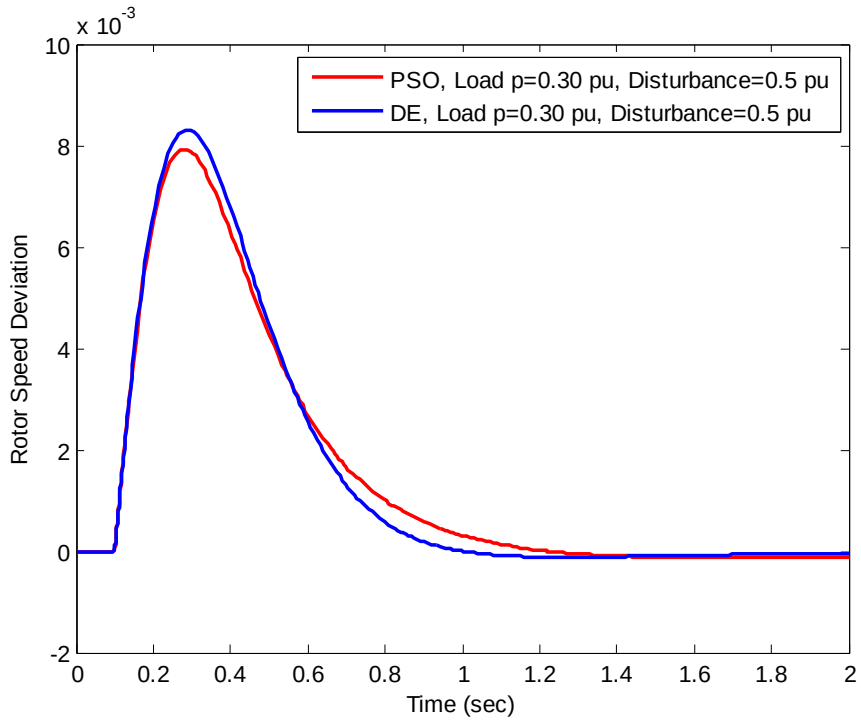

Figure 4.31: Time-domain simulation of rotor speed deviation with PSO & DE optimizers for light load with disturbance 0.5 pu

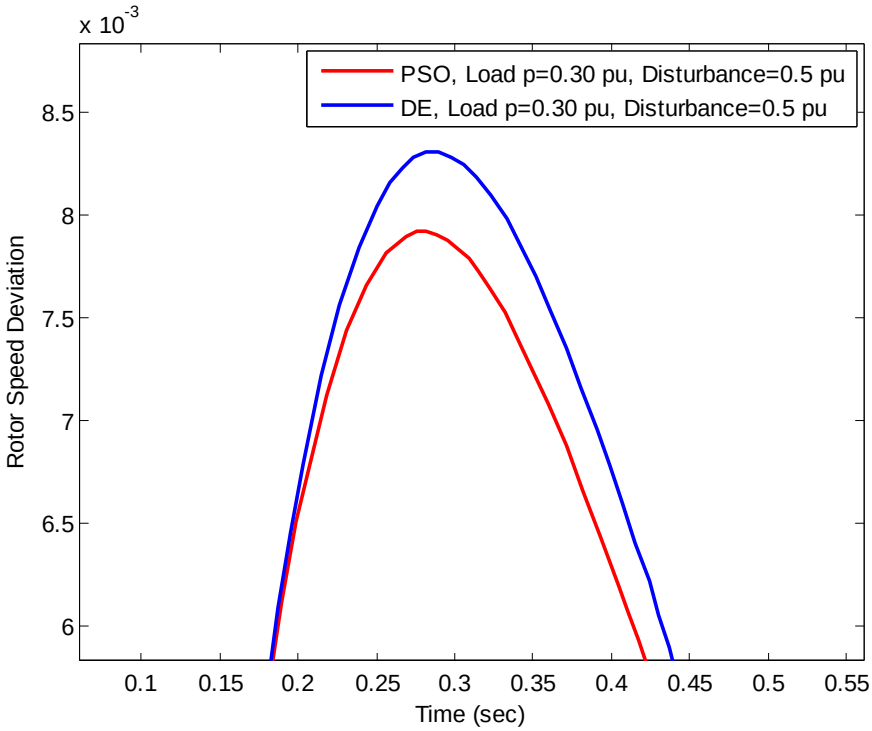

Figure 4.32: Zoom view of overshoot for Fig.4.31

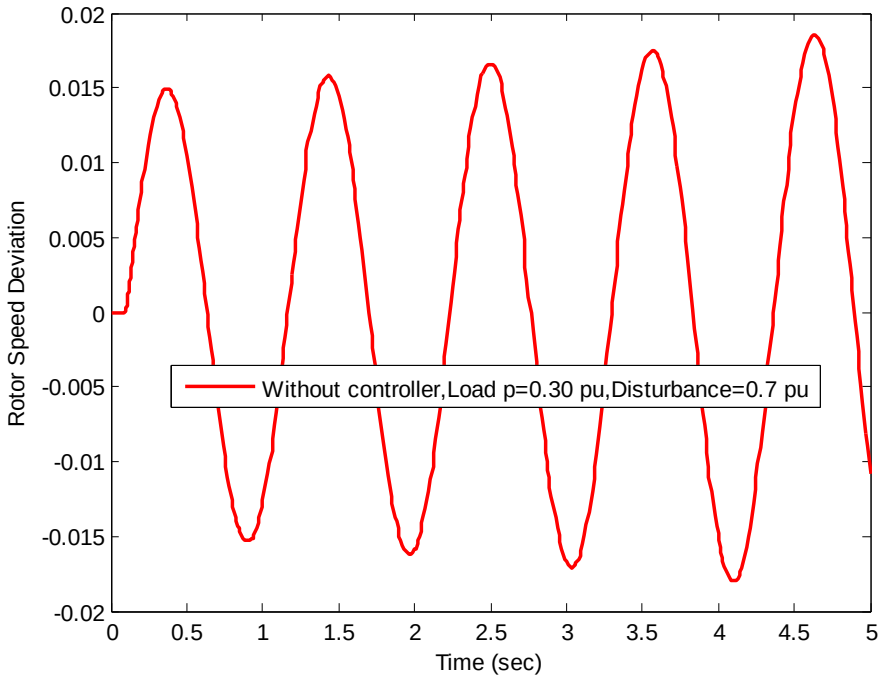

Figure 4.33: Time-domain simulation of rotor speed deviation without controller for light load with disturbance 0.7 pu

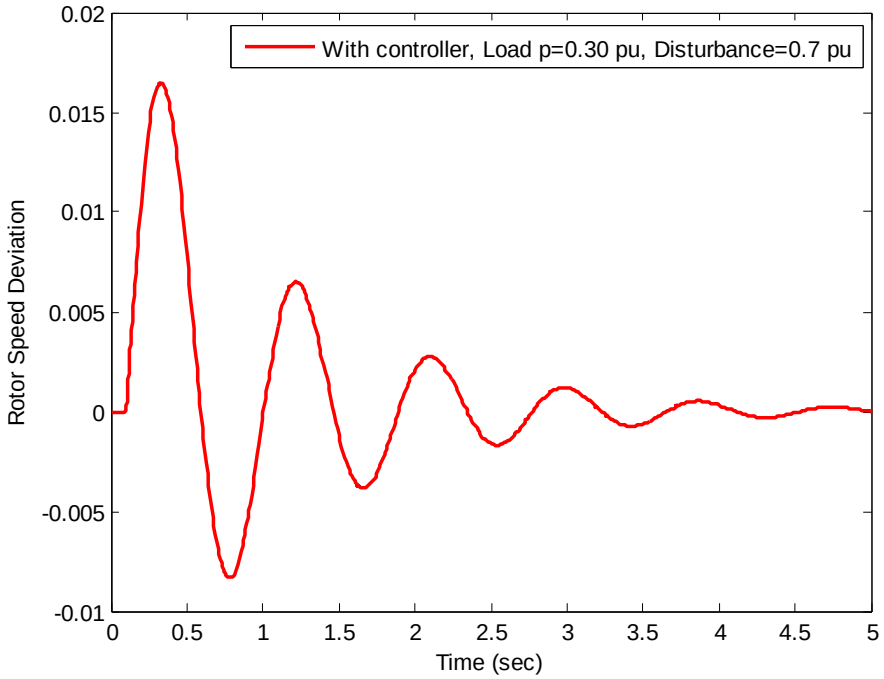

Figure 4.34: Time-domain simulation of rotor speed deviation with controller for light load with disturbance 0.7 pu

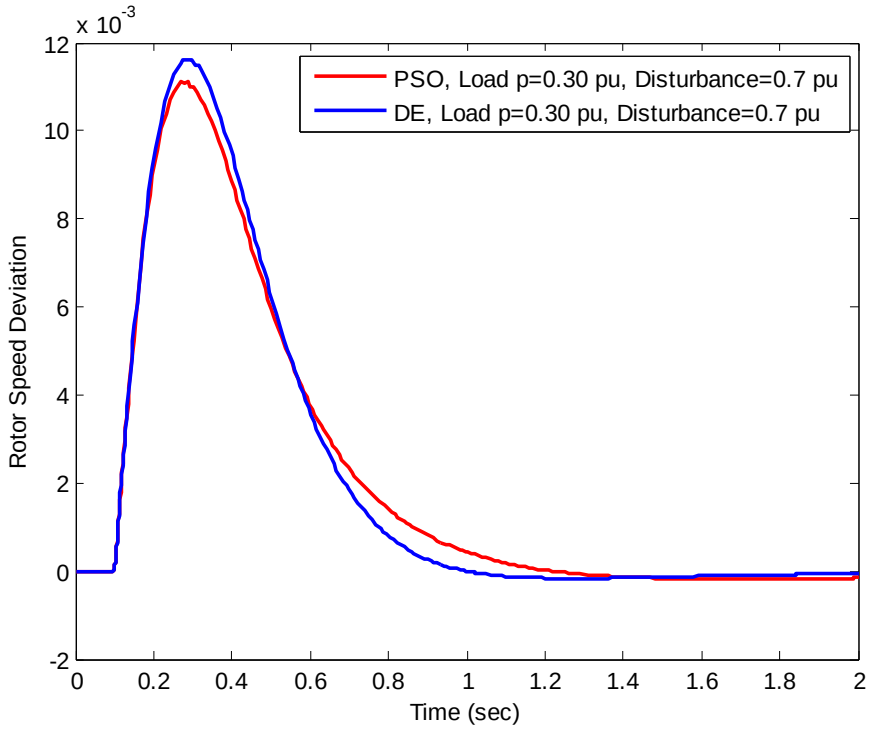

Figure 4.35: Time-domain simulation of rotor speed deviation with PSO & DE optimizers for light load with disturbance 0.7 pu

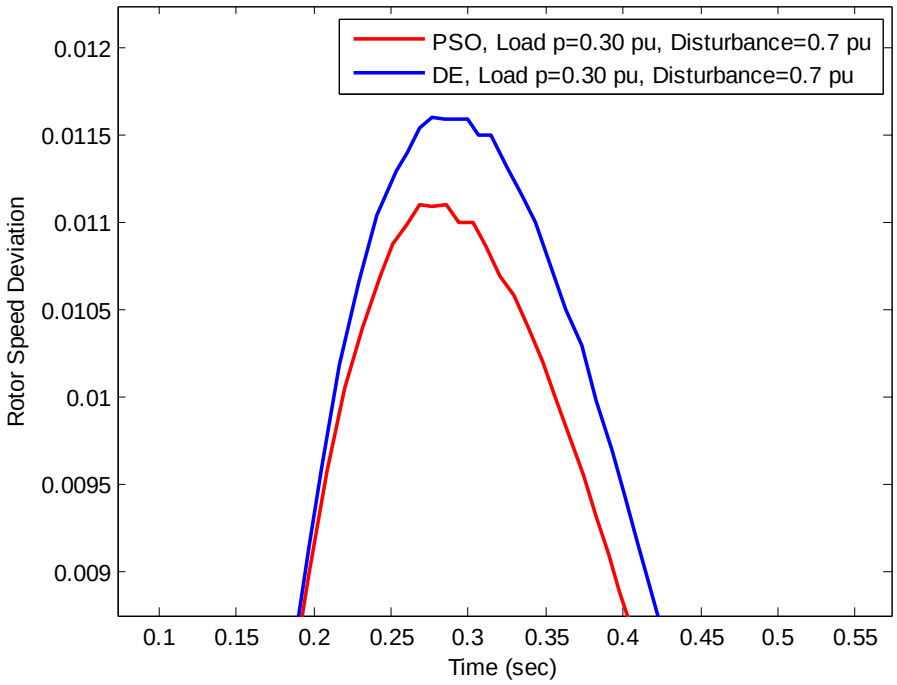

Figure 4.36: Zoom view of overshoot for Fig.4.35

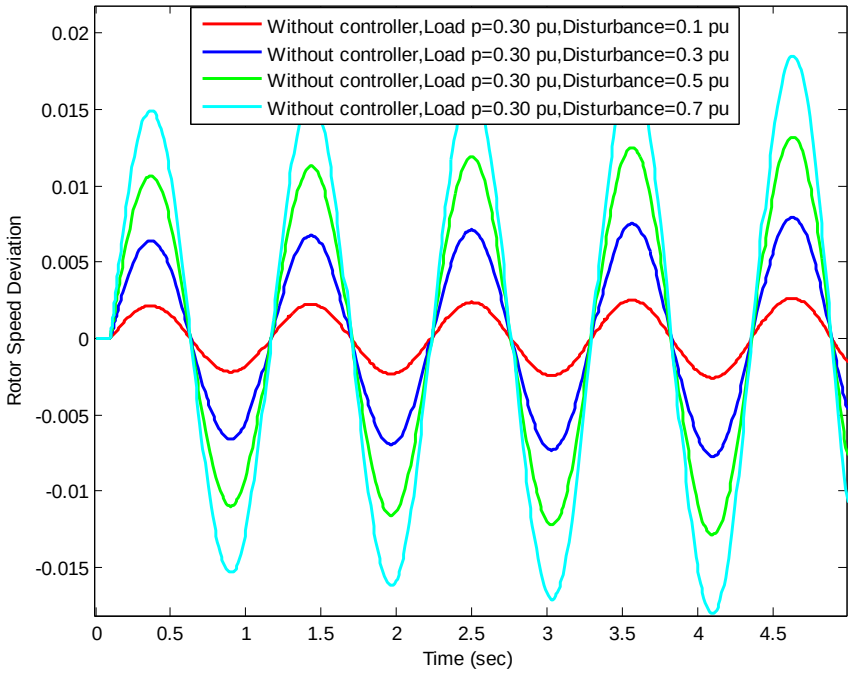

Figure 4.37: Time-domain simulation of rotor speed deviation for light load without controller for comparison of different disturbances

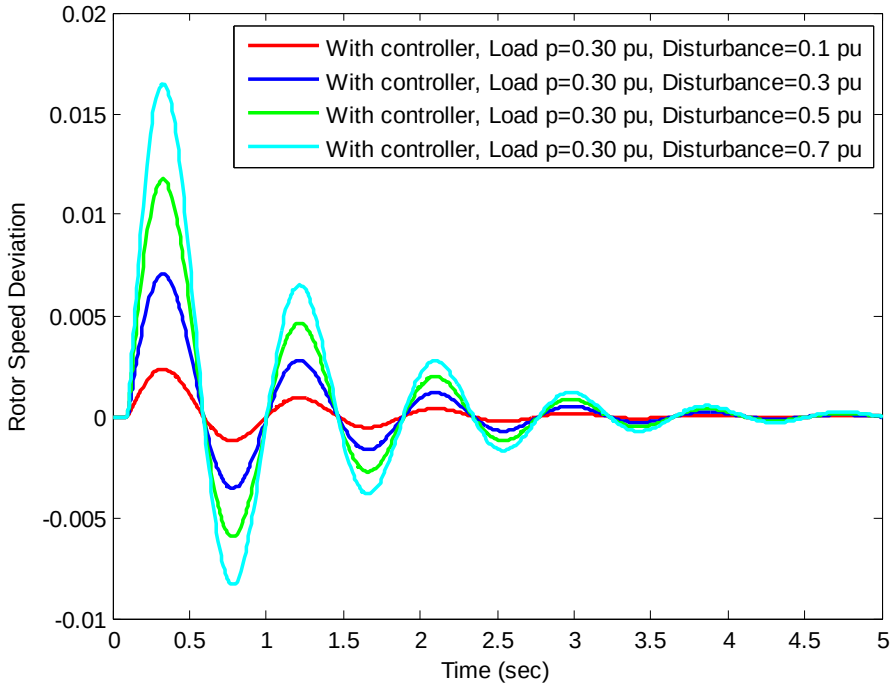

Figure 4.38: Time-domain simulation of rotor speed deviation for light load with controller for comparison of different disturbances

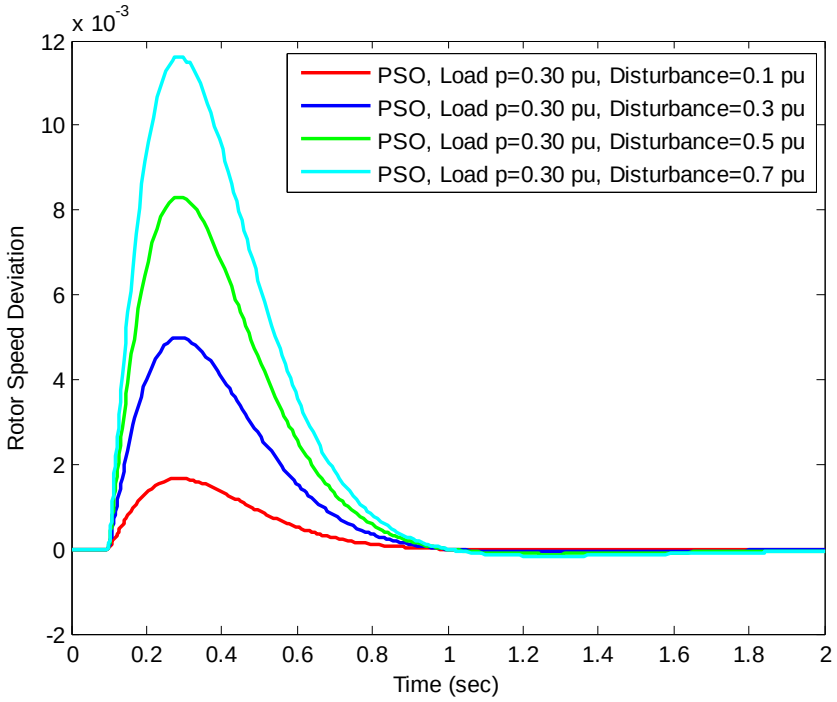

Figure 4.39: Time-domain simulation of rotor speed deviation for light load with PSO optimizer for comparison of different disturbances

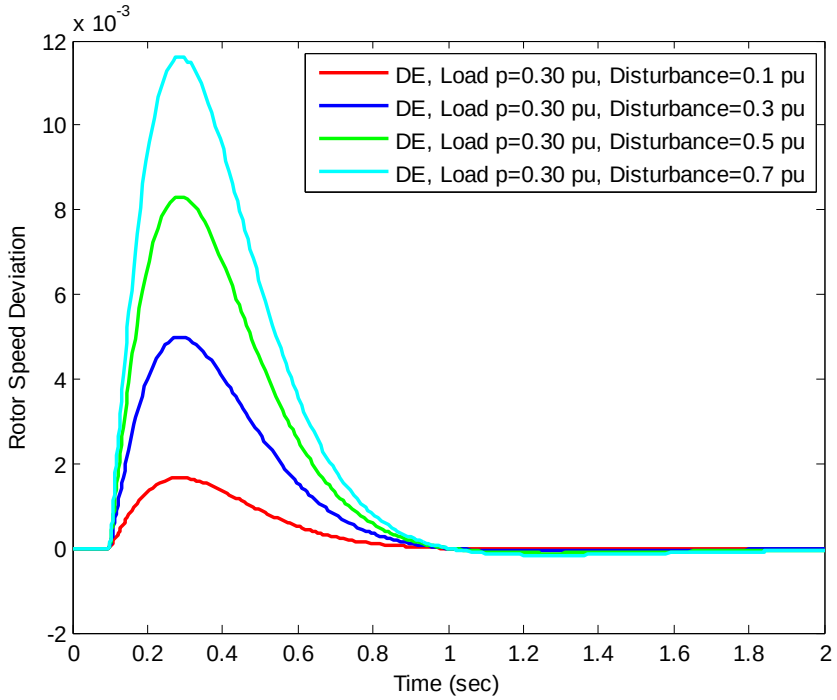

(d)

Figure 4.40: Time-domain simulation of rotor speed deviation for light load with DE optimizer for comparison of different disturbances

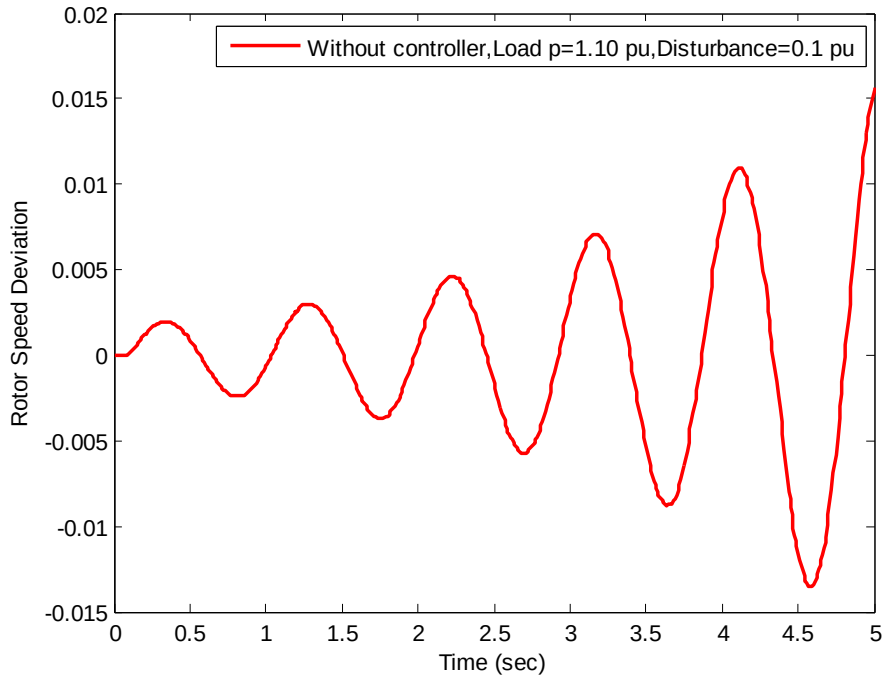

Figure 4.41: Time-domain simulation of rotor speed deviation without controller for heavy load with disturbance 0.1 pu

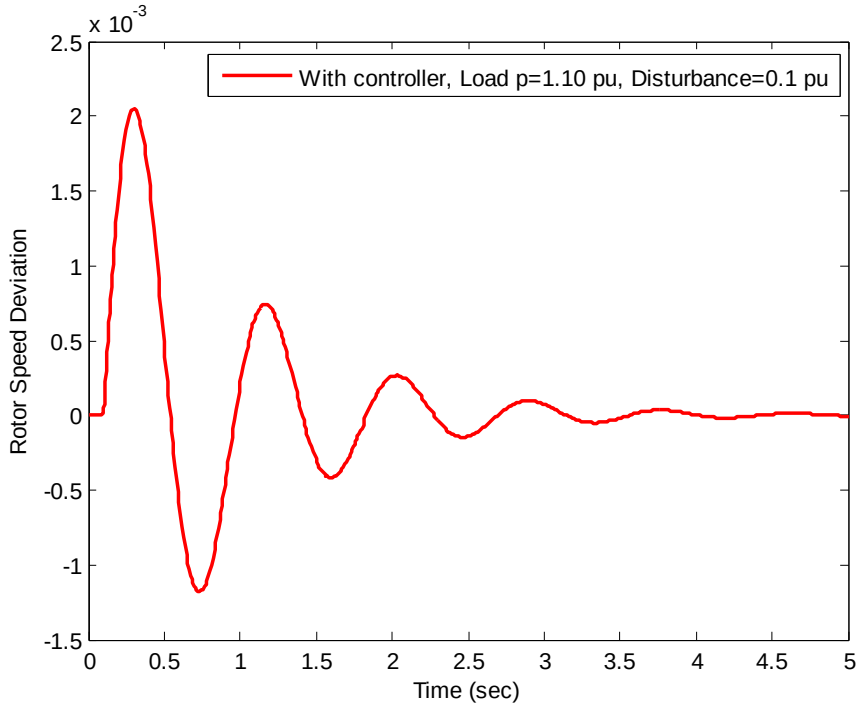

Figure 4.42: Time-domain simulation of rotor speed deviation with controller for heavy load with disturbance 0.1 pu

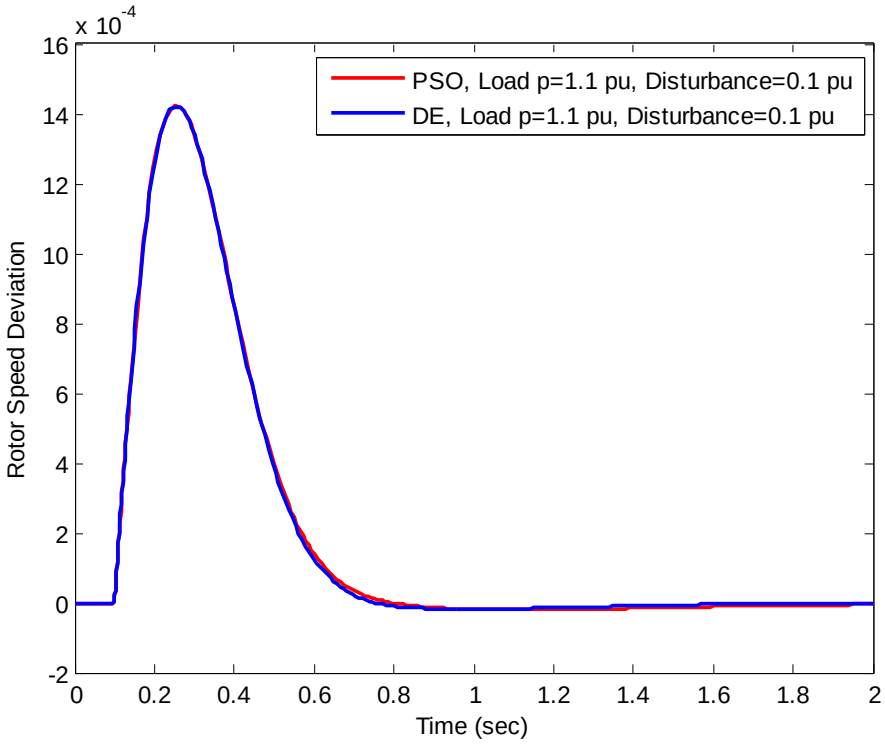

Figure 4.43: Time-domain simulation of rotor speed deviation with PSO & DE optimizers for heavy load with disturbance 0.1 pu

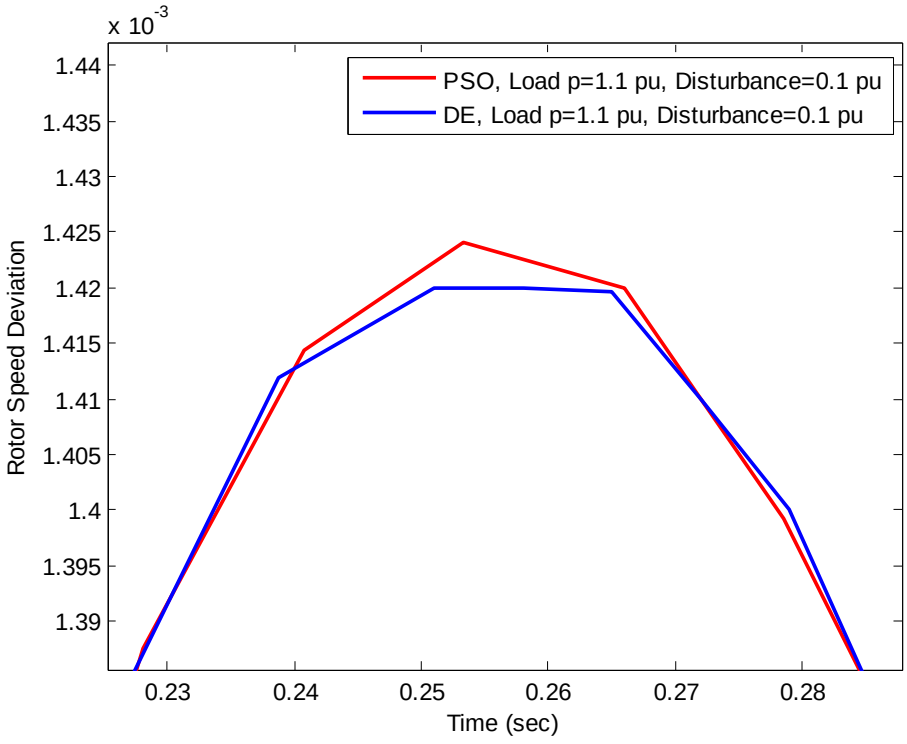

Figure 4.44: Zoom view of overshoot for Fig.4.43

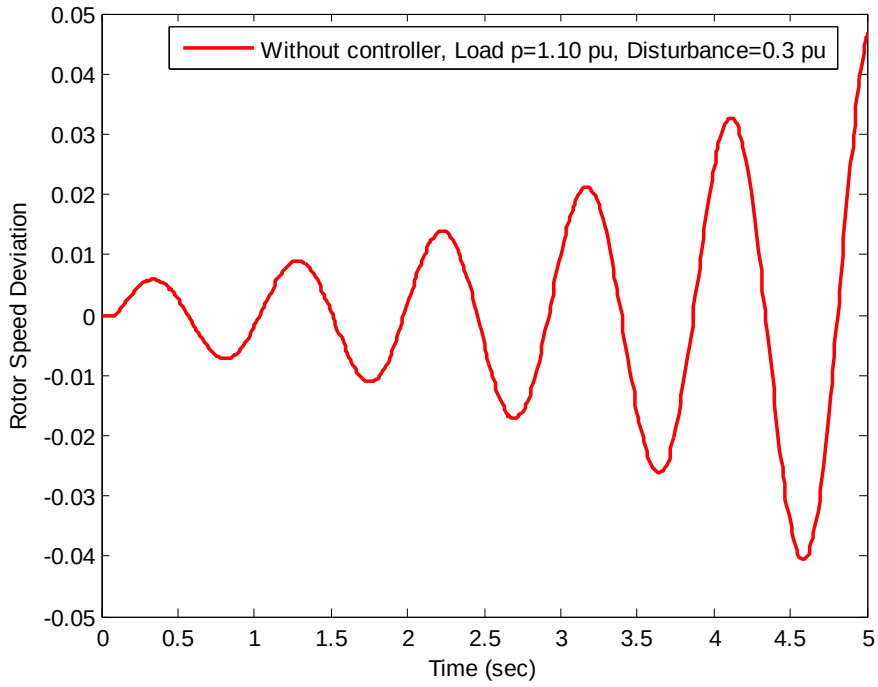

Figure 4.45: Time-domain simulation of rotor speed deviation without controller for heavy load with disturbance 0.3 pu

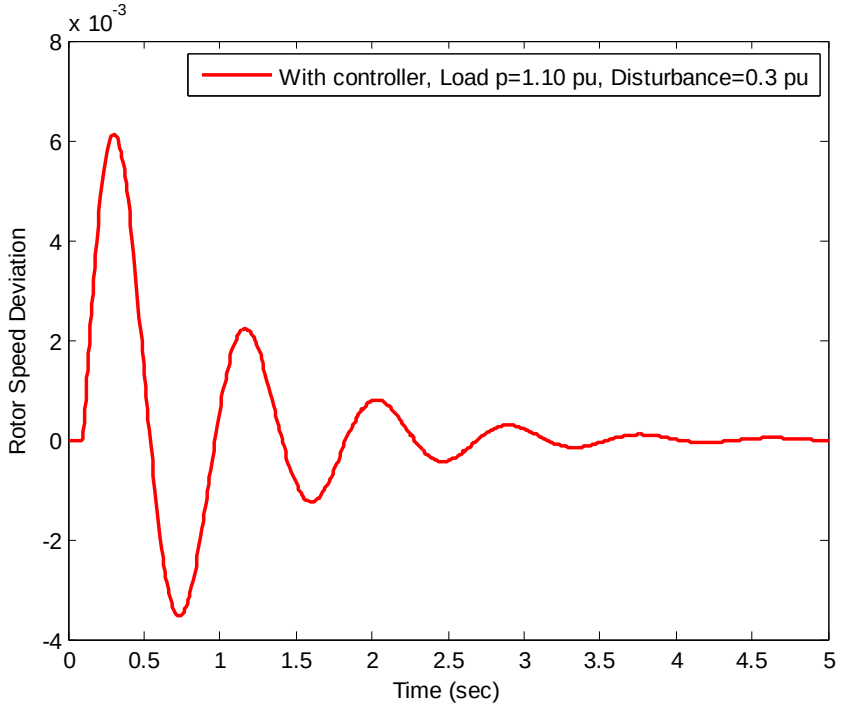

Figure 4.46: Time-domain simulation of rotor speed deviation with controller for heavy load with disturbance 0.3 pu

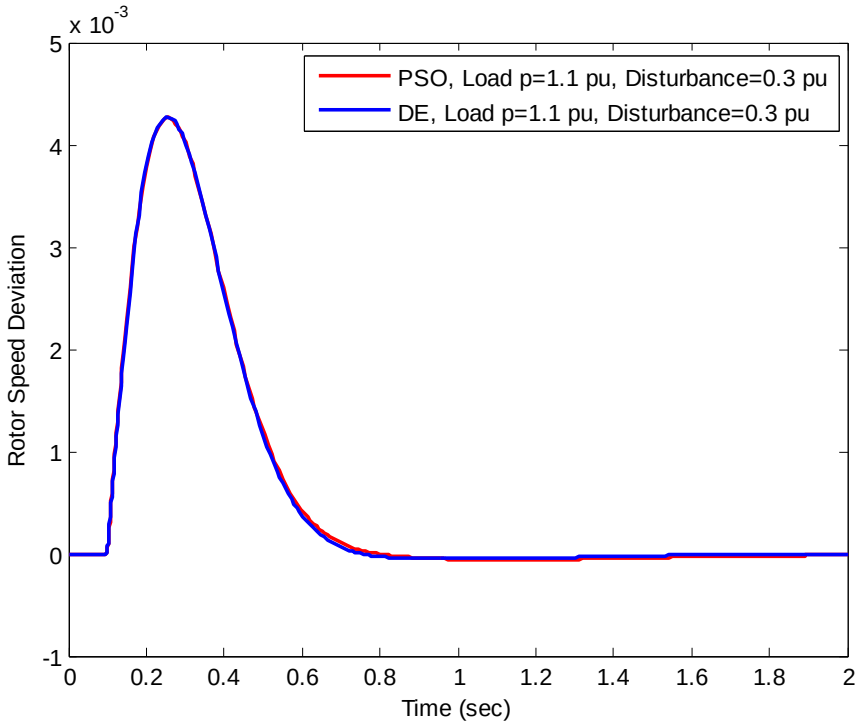

Figure 4.47: Time-domain simulation of rotor speed deviation with PSO & DE optimizers for heavy load with disturbance 0.3 pu

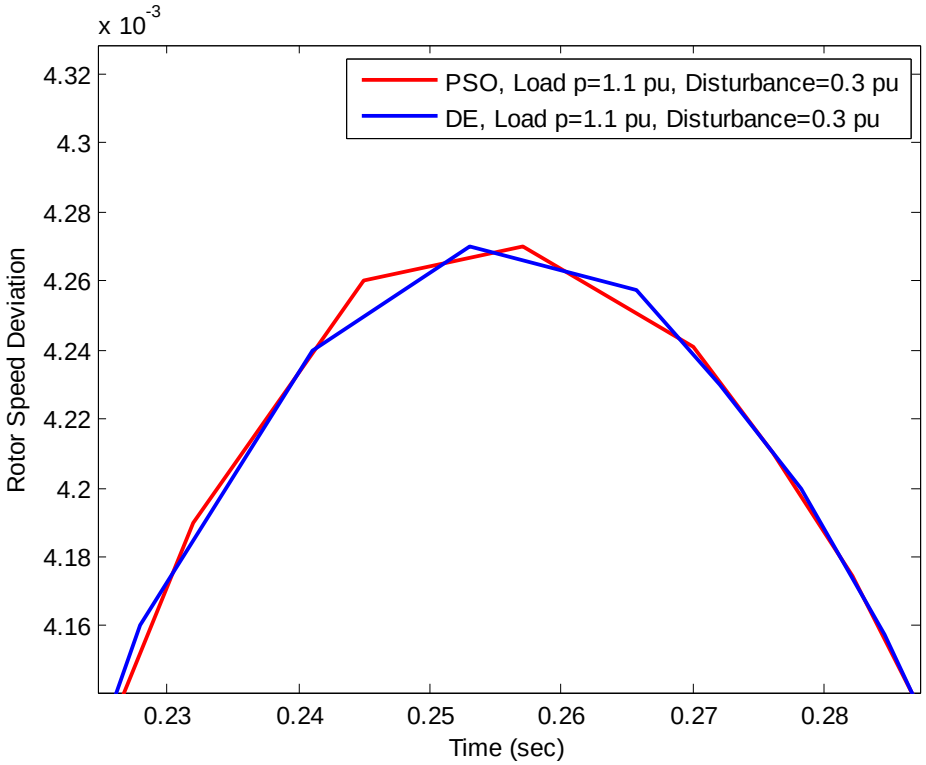

Figure 4.48: Zoom view of overshoot for Fig.4.47

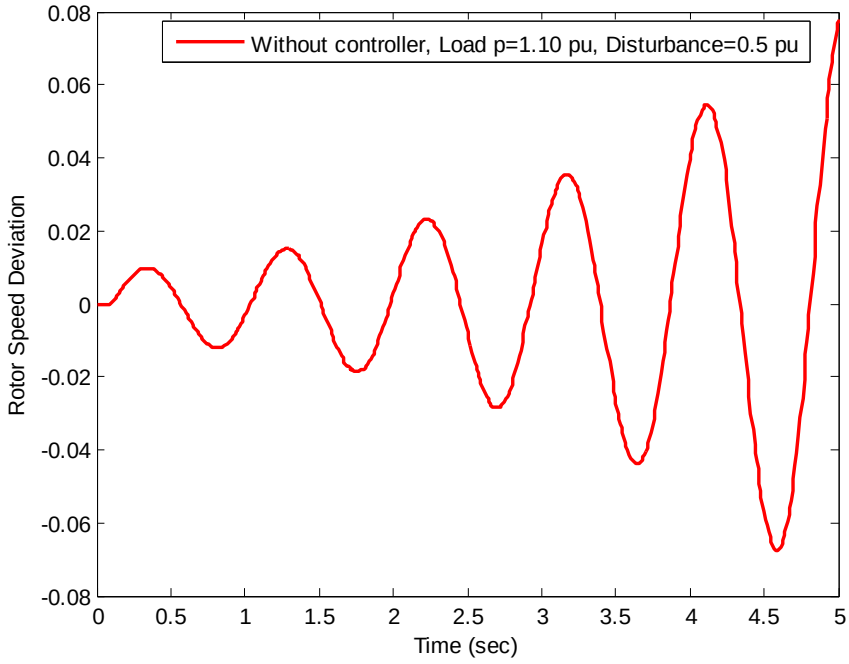

Figure 4.49: Time-domain simulation of rotor speed deviation without controller for heavy load with disturbance 0.5 pu

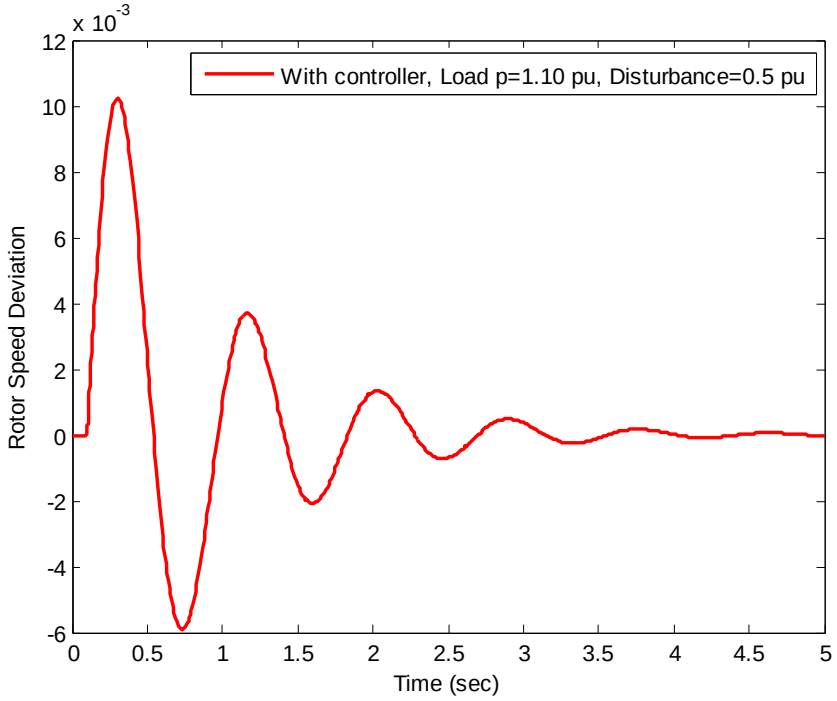

Figure 4.50: Time-domain simulation of rotor speed deviation with controller for heavy load with disturbance 0.5 pu

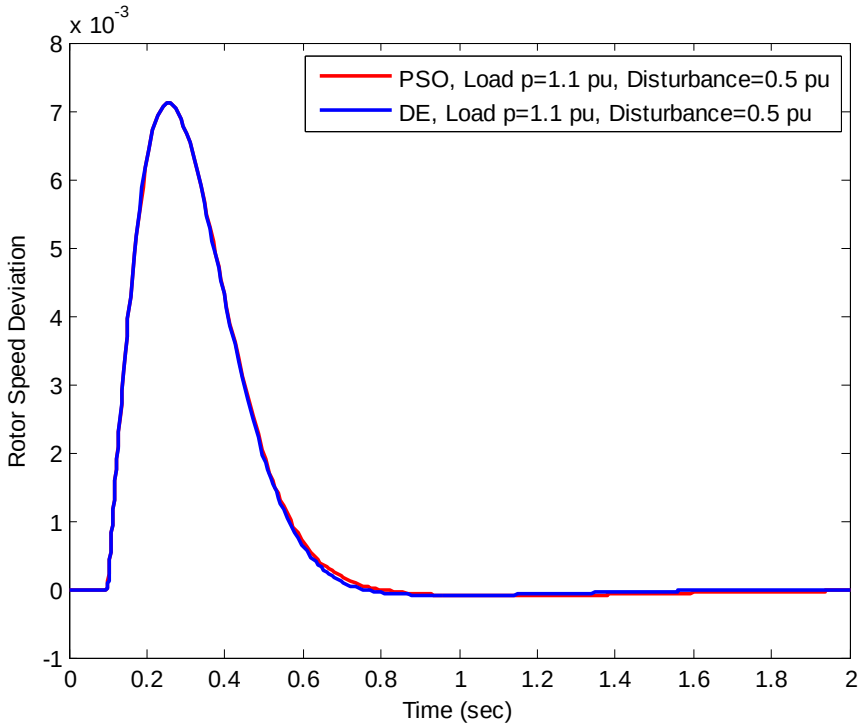

Figure 4.51: Time-domain simulation of rotor speed deviation with PSO & DE optimizers for heavy load with disturbance 0.5 pu

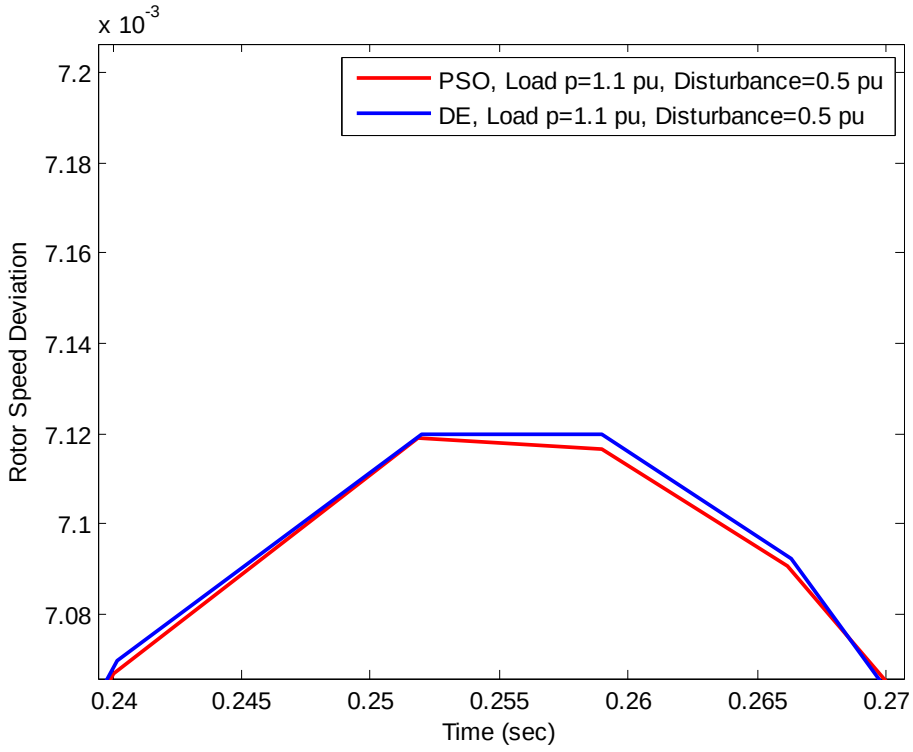

Figure 4.52: Zoom view of overshoot for Fig.4.51

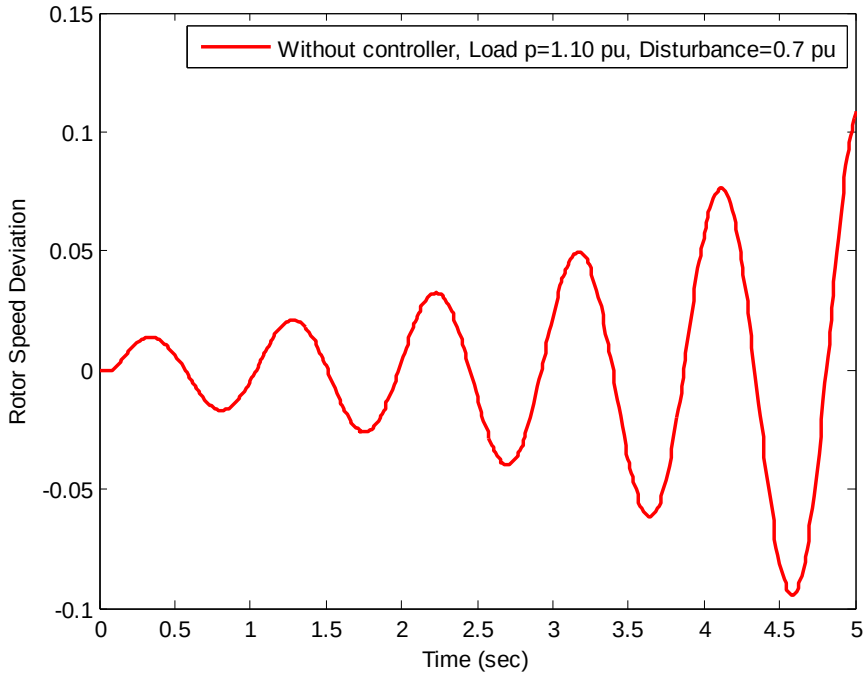

Figure 4.53: Time-domain simulation of rotor speed deviation without controller for heavy load with disturbance 0.7 pu

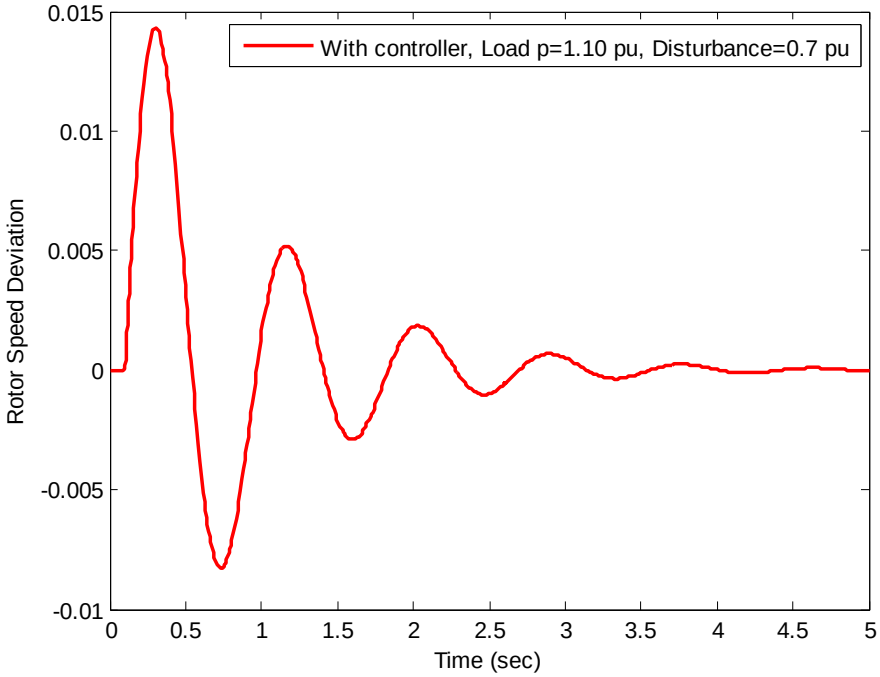

Figure 4.54: Time-domain simulation of rotor speed deviation with controller for heavy load with disturbance 0.7 pu

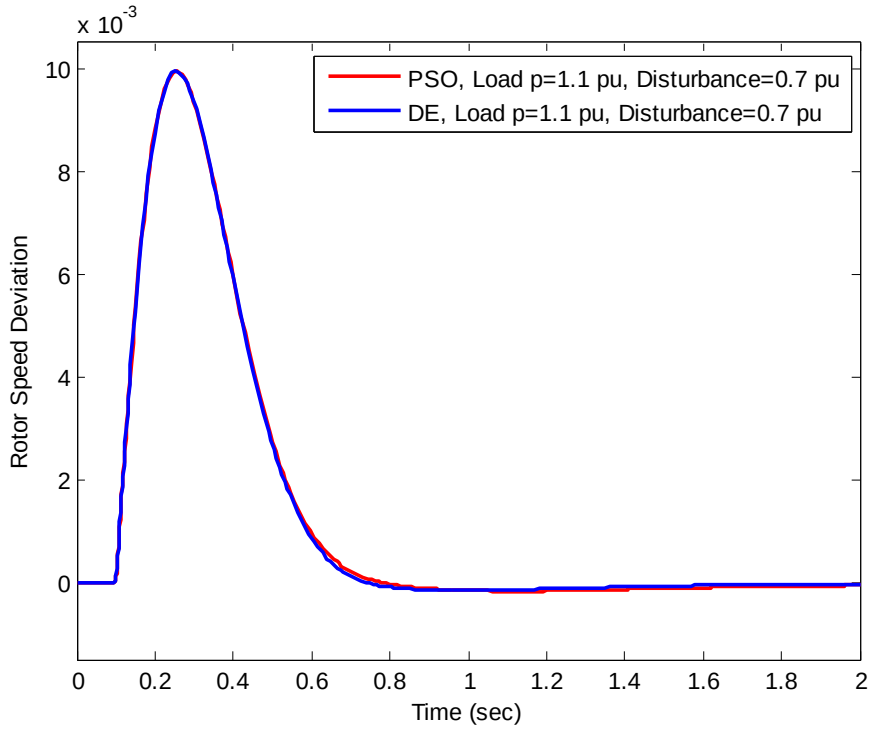

Figure 4.55: Time-domain simulation of rotor speed deviation with PSO & DE optimizers for heavy load with disturbance 0.7 pu

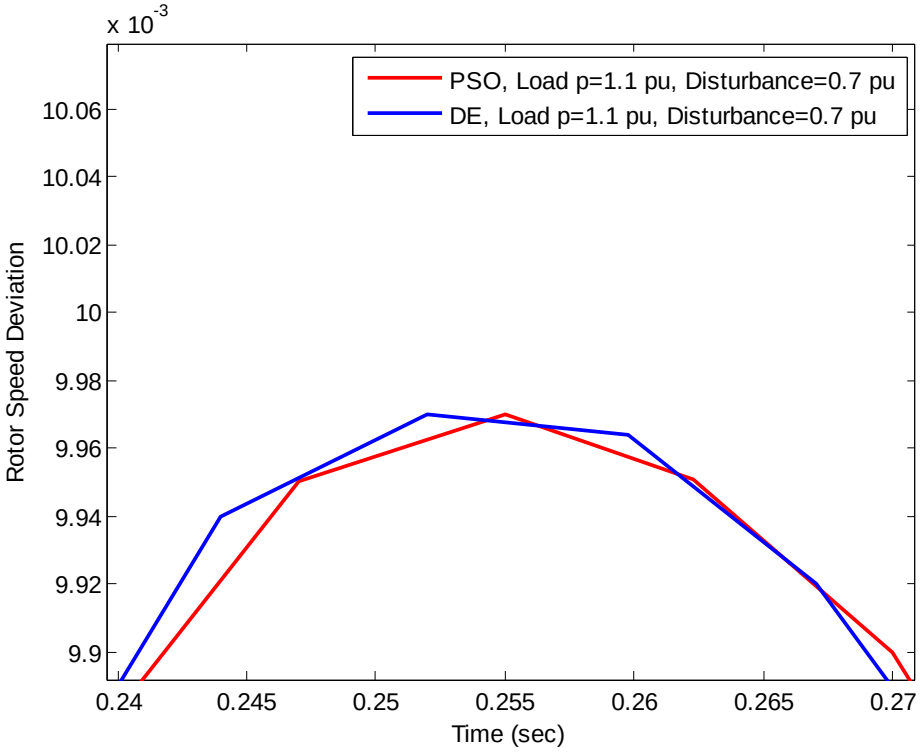

Figure 4.56: Zoom view of overshoot for Fig.4.55

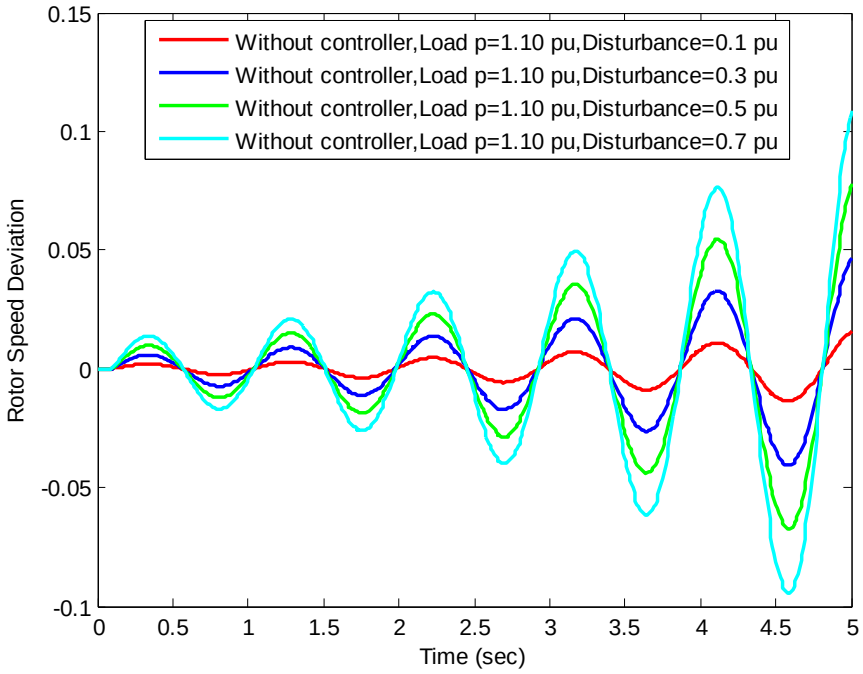

Figure 4.57: Time-domain simulation of rotor speed deviation for heavy load without controller for comparison of different disturbances

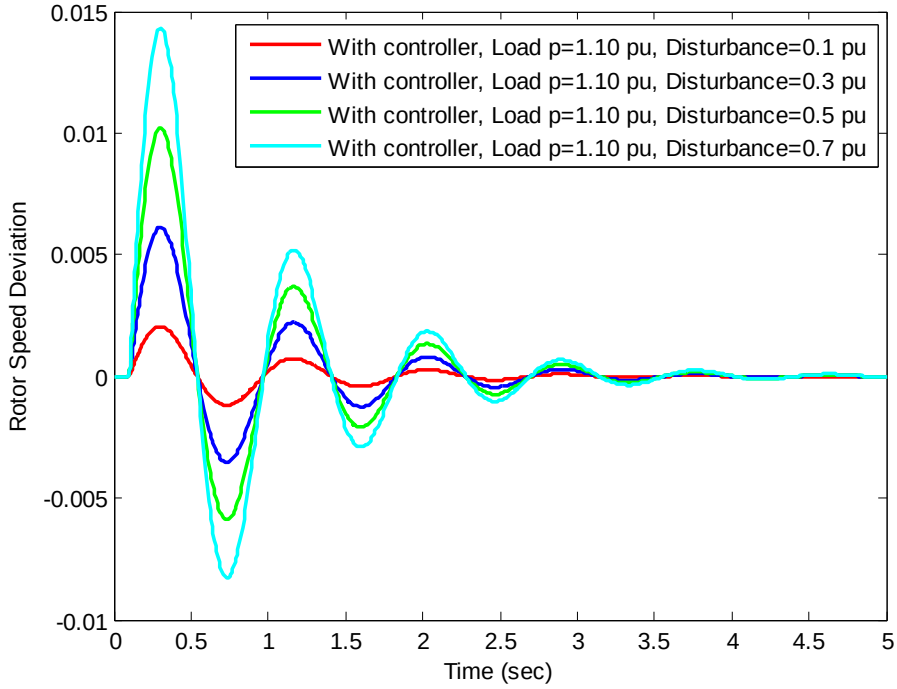

Figure 4.58: Time-domain simulation of rotor speed deviation for heavy load with controller for comparison of different disturbances

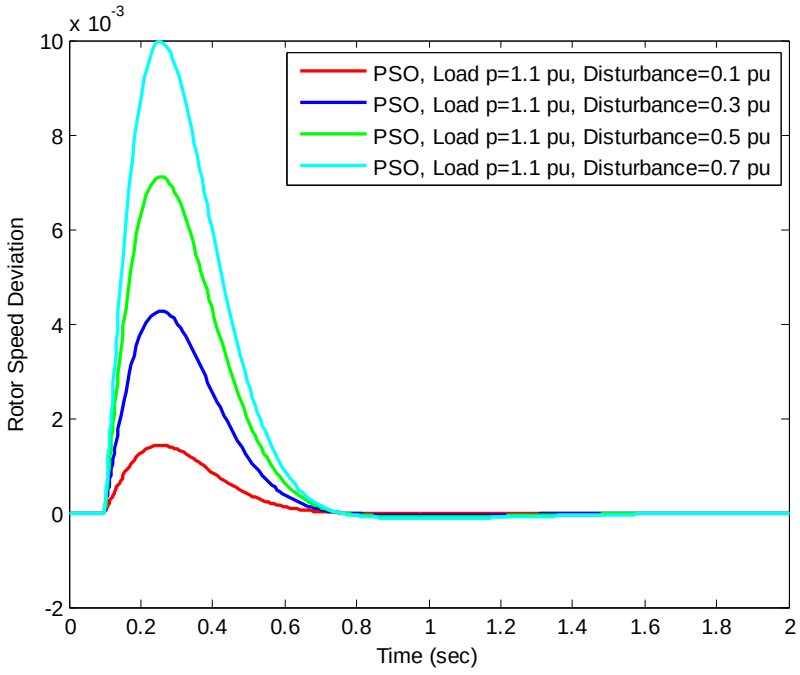

Figure 4.59: Time-domain simulation of rotor speed deviation for heavy load with PSO optimizer for comparison of different disturbances

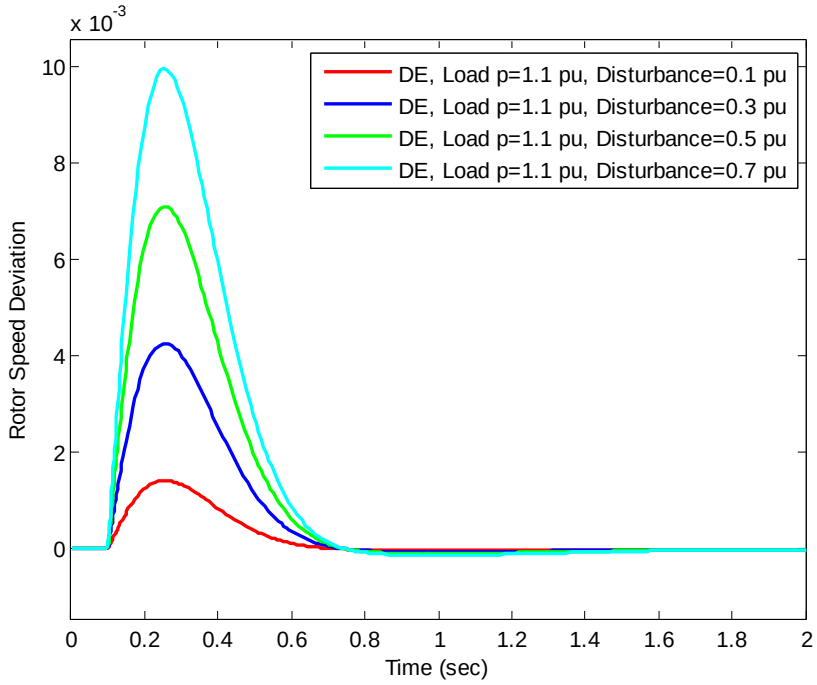

(d)

Figure 4.60: Time-domain simulation of rotor speed deviation for heavy load with DE optimizer for comparison of different disturbances

4.4 Critical analysis of the simulation results

It is investigate from Fig. 4.5, 4.10 & 4.15 that for different disturbances the introduced oscillations are also different such as for lowest disturbance (0.1 pu) the pick value of oscillation is also lowest and for highest disturbance (0.7 pu) the pick value of oscillation is also highest. Further, clearly shown that all the disturbances from 0.1 to 0.7 pu are controlled successfully by the optimally tuned controller. It is also observed from Table 4.2 that the overshoots of DE are identical to PSO for various load conditions except light load and the settling times of DE are smaller (better) than PSO for various load conditions except nominal load. Although under nominal load DE requires slightly higher settling time than PSO and under light load the overshoot of DE is higher (worst) than PSO, DE exhibits best performance in terms of overall results from all loading scenarios.

Table 4.2: Settling time and overshoot

Loading condition	Optimizer	Settling time (sec)	Overshoot (p.u.)
Nominal load	PSO	0.8464	0.0015
	DE	0.8659	0.0015
Light load	PSO	1.9390	0.0012
	DE	1.8283	0.0013
Heavy load	PSO	1.3634	0.0015
	DE	1.3225	0.0015

4.5 Quantitative analysis

In this section, the quantitative analysis is performed between PSO and DE optimizers in order to compare the performance of them.

Table 4.3: Fitness values and elapsed time

Parameters	Best result		Average result		Worst result	
	PSO	DE	PSO	DE	PSO	DE
Elapsed time	12.3099 sec	11.4467 sec	13.1922 sec	12.3845 sec	14.9658 sec	13.9008 sec
Best fitness value	-91401.544	-91418.210	-91419.016	-91420.605	-91422.187	-91422.196

The outcomes of the quantitative analysis these optimizers in terms of computational (elapsed) time and best fitness value are illustrated in Table 4.2. It is observed that the elapsed time required for DE is smaller than PSO and the best fitness value required for DE is also higher than PSO in all cases such as best, average and worst conditions. Hence, it is revealed that DE is better in terms of both elapsed time and fitness value, which supports the result obtained in time-domain simulation.

4.6 Non-Parametric statistical analysis

To strengthen the result obtained from the eigenvalue and time domain analyses, single sample Kolmogorov-Smirnov test is performed for 30 independent test runs and the data sets are shown in Table 4.4.

Table 4.4: Single sample Kolmogorov-Smirnov test result

Normal Parameters		PSO	DE
Number of Runs		30	30
Mean		-91419.0168	-91420.6055
Standard Deviation		5.08527	1.01004
Most Extreme Differences	Absolute	0.266	0.154
	Positive	0.243	0.154
	Negative	-0.266	-0.081
Kolmogorov-Smirnov -Z		0.170	0.188
Asymp. Sig. (2-tailed)		0.000	0.068

It is observed that the mean value of DE is larger (better) than PSO. Again, according to the standard deviation and the most extreme differences of DE are smaller (better) than PSO. Then, in terms of the *p* value (Asymp. Sig.2-tailed) for PSO and DE accepts H_1, implies that they do not follow normal distribution.

Chapter 5
Conclusion and Future Scopes

5.1 Conclusion

In this thesis, the effectiveness of PSO and DE optimizers has been investigated. The optimizers have been used to tune the controller parameters in SMIB system. The eigenvalue analysis in open loop condition has been performed to find out the unstable mode (EM mode). The controllability test has been done for selecting the most appropriate control signal of the lead-lag controller. Further, the PSO and DE has been employed to optimize the controller parameters that improve the negatively damped (-0.0599) EM mode by shifting all the eigenvalues to the left half of S-plane. The settling time and overshoot have been investigated by the time domain simulation in order to find out the best results for the system in nominal, light & heavy load conditions with various fault disturbances. Comparative study reveals that to mitigate LFO depicted in time domain characteristics, DE optimizer is better than PSO in terms of overshoot and settling time. The eigenvalue analysis in closed loop condition shows that DE tuned controller produces highest damping effect (0.999999995) and less settling time average (1.3389 *sec*.) than PSO tuned controller. Furthermore, to find out the overall performance of the optimizers, quantitative analysis has been carried out which reveal that in terms of fitness value of DE is larger (better) and the elapsed time of DE is smaller (better) than PSO.

5.2 Future scopes

To achieve high efficiency and high reliability of power system, many control strategies based on advanced control theories have been introduced. Model Predictive Control (MPC) is the only practical control method that takes account of system constraints explicitly and the only advanced control method to have been adopted widely in industry. To the extension of this research work, MPC can be used as controller that usually uses an online optimization in real time to determine control signals. The solution to optimization problem can be formulated with the help of the system model. At each control interval, an optimization algorithm can be justified to determine

the system dynamics by computing a sequence of control input values satisfying the control specifications. LFO mitigation for Multi-Machine system can be implemented for the same loading scenario. Advanced Fuzzy Logic based approach for the optimal design of gain parameters for the IPFC based damping controller can be implemented. The problem of selecting optimized parameter for damping controller can be formulated by optimization problem with some adaptive controller. In future the performance of the proposed IPFC based damping controller can be compared to phase compensation method.

References

[1] A. M. Vural and M. S. Hamad, "Comparison of dynamic performances of ipfc, upfc and back to back hvdc transmission on local and inter-area oscillation damping in power systems," *International Conference on Electrical and Electronics Engineering,* vol. 9, no. 18, pp. 31-35, 2018.

[2] N. M. R. Santos, O. P. Dias and V. F. Pires, "Use of an interline power flow controller model for power flow analysis" *International Conference on Advances in Energy Engineering,* vol. 14, pp. 2096-2101, 2011.

[3] A. M. Parimi, I. Elamvazuthi, A. V. P. Kumar and V. Cherian "Fuzzy logic based control for ipfc for damping low frequency oscillations in multi machine power system," *Industrial And Commercial Power Systems/Petroleum And Chemical Industry Conference (ICPSPCIC),* vol. 3, no. 15, pp. 32-36, 2015.

[4] M. O. Hassan and A. K. Alhaj, "Analysis and performance of inter line power flow controller (ipfc) for damping low frequency oscillations," *International Journal of Advance Engineering and Research Development,* vol. 5, pp. 14-20, 2018.

[5] H. Shayeghi, H. Shayanfar, S. Jalilzadeh and A. Safari, "Design of output feedback upfc controller for damping of electromechanical oscillations using pso," *Energy Conversion and Management,* vol. 50, pp. 2554-2561, 2009.

[6] M. V. Reddy, B. P. Muni and A. V. R. S. Sarma, "Enhancement of transient stability in fourteen bus system using interline power flow controller," International *Conference on Computing Methodologies and Communication (ICCMC),* vol. 8, no. 17, pp. 1145-1150, 2017.

[7] B. V. R. Reddy, Y. V. S. Reddy and P. Sujatha, "Optimal placement of interline power flow controller (ipfc) to enhance voltage stability," *Conference on Power, Control, Communication and Computational Technologies for Sustainable Growth (PCCCTSG),* vol. 2, no. 15, pp. 78-84, 2015.

[8] T. V. Charan, P. A. Manga, “Placing ipfc at multiple generator connected grid for reducing short circuit current*,” Industrial and Commercial Power Systems/Petroleum and Chemical Industry Conference (ICPSPCIC),* vol. 3, no. 15, pp. 90-95, 2015.

[9] A. Ghorbani, S. Y. Ebrahimi and M. Ghorbani, “Modeling generalized interline power-flow controller (gipfc) using 48-pulse voltage source converters,” *Journal of Electrical Systems and Information Technology (JESIT),* pp. 1-15, 2017.

[10] A. Younesi, H. Shayeghi and M. Moradzadeh, “Application of reinforcement learning for generating optimal control signal to the ipfc for damping of low frequency oscillations,” *WILEY,* pp. 1-23, 2017.

[11] A. Keri, A. Mehraban, X. Lombard, A. Eiriachy, and A. Edris, “Unified power flow controller (upfc) modeling and analysis,” *IEEE Transactions on Power Delivery,* vol. 14, no. 2, pp. 648-654, 1999.

[12] M. Kothari and N. Tambey, “Unified power flow controller (upfc) based damping controllers for damping low frequency oscillations in a power system,” *IE (I) Journal-EL,* vol. 84, pp. 35-41, 2003.

[13] G. Reed, R. Pape, and M. Takeda, “Advantages of voltage sourced converter (vsc) based design concepts for facts and hvdc-link applications,” *Power Engineering Society General Meeting, 2003, IEEE,* vol. 3, pp. 1816-1821, 2003.

[14] L. Gyugyi, K. K. Sen and C. D. Schauder, “The interline power flow controller: a new approach to power flow management in transmission systems,” *IEEE Trans. on Power Delivery,* vol. 14, pp. 1115-1123, 1999.

[15] N. G. Hingorani and L. Gyugyi, “Understanding facts: concepts and technology of flexible ac transmission systems” *IEEE Press,* chap. 1-13, pp. 452, 2000.

[16] N. M. R. Santos, V. M. F. Pires and R. M. G. Castro, “A new model to incorporate unified power flow controllers in power flow studies” *IEEE PES Transmission and Distribution Conference and Exhibition,* pp. 8555-8563, 2006.

[17] Y. Zhang, Y. Zhang and C. Chen, “A novel power injection model of IPFC for power flow analysis inclusive of practical constraints” *IEEE Transactions on Power Systems,* vol. 21, no. 4, pp. 1550-1556, 2006.

[18] J. V. Milanovic and Y. Zhang, “Modeling of facts devices for voltage sag mitigation studies in large power systems,” *IEEE transactions on power delivery,* vol. 25, no. 4, pp. 3044-3052, 2010.

[19] A. V. N. Babu, S. Sivanagaraju, C. Padmanabharaju and T. Ramana, “Multi-line power flow using interline power flow controller (ipfc) in power transmission systems” *World Academy of Science, Engineering and Technology, International Journal of Electrical, Computer, Energetic, Electronic and Communication Engineering,* vol. 4, no. 3, pp. 577-581, 2010.

[20] F. Milano, “An open source power system analysis toolbox," *IEEE Transactions on Power systems,* vol. 20, no. 3, pp. 1199-1206, 2005.

[21] F. Milano, “Psat: power system analysis toolbox, version 2.0. 0-beta,” 2007.

[22] D. Lee, “Ieee recommended practice for excitation system models for power system stability studies (ieee std 421.5-1992),” *Energy Development and Power Generating Committee of the Power Engineering Society,* vol. 95, no. 96, 1992.

[23] P. Dalgaard, “introductory statistics with r,” *Springer Science & Business Media,* 2008.

[24] A. Mohanty, S. Patra and P. K. Ray, “Robust fuzzy-sliding mode based upfc controller for transient stability analysis in autonomous wind-diesel-pv hybrid system,” *IET Generation, Transmission & Distribution,* vol. 10, pp. 1248-1257, 2016.

[25] R. Storn and K. Price, “Differential evolution - a simple and efficient heuristic for global optimization over continuous spaces,” *Journal of global optimization,* vol. 11, no. 4, pp. 341-359, 1997.

[26] A. Ahmed, M. M. H. Galib, S. M. K. Zaman, and G. Sarowar, “An optimization methodology of susceptance variation using lead-lag controller for grid connected sig based wind generator system,” *Journal of the Franklin Institute,* vol. 355,no. 1, pp. 197-217, 2018.

[27] M. T. Khosroshahi, F. M. Kazemi, M. R. J. Oskuee and S. N. Ravadanegh, “Coordinated and uncoordinated design of lfo damping controllers with ipfc and pss using ica and sfla,” *Springer, Journal of Central South University,* vol. 22, pp. 3418-3426, 2015.

[28] Y. A. Magid, M. Abido, S. Al-Baiyat and A. Mantawy, “Simultaneous stabilization of multi machine power systems via genetic algorithms,” *IEEE transactions on Power Systems,* vol. 14, no. 4, 1999.

[29] M. Abido and Y. A. Magid, “Coordinated design of a pss and an svc-based controller to enhance power system stability,” *International Journal of Electrical Power & Energy Systems,* vol. 25, no. 9, pp. 695-704, 2003.

[30] H. Wang and W. Du, “Analysis and damping control of power system low frequency oscillations,” *Springer,* et al., 2016.

[31] N. G. Hingorani, “High power electronics and flexible ac transmission system,” *Proceedings of the American Power Conference,* vol. 50, 1988.

[32] E. B. Martinez and C. A. Camacho, “Technical comparison of facts controllers in parallel connection,” *Journal of Applied Research and Technology,* vol. 15, pp. 36-44, 2017.

[33] S. Chirantan, R. Jena, S. Swain and P. Panda, “Comparative analysis of statcomand tcsc facts controller for power profile enhancement in a long transmission line,” *IEEE, International Conference on Communication and Electronics Systems (ICCES),* pp. 407-413, 2017.

[34] C. A. Canizares, N. Mithulananthan, F. Milano and J. Reeve, “Linear performance indices to predict oscillatory stability problems in power systems,” *IEEE Transactions on Power Systems,* vol. 19, no. 2, pp. 1104-1114, 2004.

[35] K. Prasertwong, N. Mithulananthan and D. Thakur, “Understanding low frequency oscillation in power systems,” *International Journal of Electrical Engineering Education,* vol. 47, no. 3, pp. 248-262, 2010.

[36] A. Mishra and G. V. N. Kumar, “Congestion management of power system with interline power flow controller using disparity line utilization factor and multi-objective differential evolution,” *CSEE Journal of Power and Energy Systems,* vol. 1, no. 3, pp. 76-85, 2015.

[37] N. Bizon, H. Shayeghi and N. M. Tabatabaei, “Analysis, control and optimal operations in hybrid power systems: advanced techniques and applications for linear and nonlinear systems,” *Springer,* 2013.

[38] B. K. Kumar, S. Singh and S. Srivastava, “Placement of facts controllers using modal controllability indices to damp out power system oscillations,” *IET Generation, Transmission & Distribution,* vol. 1, no. 2, pp. 209-217, 2007.

[39] M. E. Aboul-Ela, A. Sallam, J. D. McCalley and A. Fouad, “Damping controller design for power system oscillations using global signals,” *IEEE Transactions on Power Systems,* vol. 11, no. 2, pp. 767-773, 1996.

[40] J. Kennedy and R. Eberhart, “Particle swarm optimization,” *IEEE,* vol. 3, pp. 1942-1948, *1995*.

[41] L. Gyugyi, C. D. Schauder and K. K. Sen, “Static synchronous series compensator: a solid-state approach to the series compensation of transmission lines,” *IEEE Transactions on Power Delivery,* vol. 12, pp. 406-417, 1997.

[42] C. M. Rimvall and C. P. Jobling, “Computer-aided control system design,” *IEEE Control Systems Magazine,* vol. 13, no. 2, pp. 14-16, 1993.

[43] P. W. Sauer and M. A. Pai, “Power system dynamics and stability,” *Department of Electrical and Computer Engineering, The University of Illinois at Urbana-Champaign, 1406 W. Green St., Urbana, IL, United States,* 1998.

[44] T. Moller, R. Machiraju, K. Mueller and R. Yagel, “Evaluation and design of filters using a taylor series expansion,” *IEEE Transactions on Visualization and Computer Graphics,* vol. 3, no. 2, pp. 184-199, 1997.

[45] A. Emadi, “Modeling of power electronic loads in ac distribution systems using the generalized state-space averaging method,” *IEEE Transactions on Industrial Electronics,* vol. 51, no. 5, pp. 992-1000, 2004.

[46] K. R. Padiyar, “Power system dynamics stability and control,” *BS publications,* 2008.

[47] Z. Dong, P. Zhang, J. Ma, J. Zhao, M. Ali, K. Meng and X. Yin, “Emerging techniques in power system analysis,” *Springer Science & Business Media,* pp. 199, 2010.